2011

# Synthesis, Characterization, And Spectroscopic Studies Of Lanthanide Complexes With Potential For Increased Sensitization And Luminescent Enhancement

Kendra Evette Whitehead
*North Carolina Agricultural and Technical State University*

# Synthesis, Characterization, and Spectroscopic Studies of Lanthanide Complexes with Potential for Increased Sensitization and Luminescent Enhancement

Kendra Evette Whitehead

North Carolina A&T State University

A thesis submitted to the graduate faculty

in partial fulfillment of the requirements for the degree of

MASTER OF SCIENCE

Department: Chemistry

Major: Chemistry

Major Professor: Dr. Zerihun Assefa

Greensboro, North Carolina

2011

School of Graduate Studies
North Carolina Agricultural and Technical State University

This is to certify that the Master's Thesis of

Kendra Evette Whitehead

has met the thesis requirements of
North Carolina Agricultural and Technical State University

Greensboro, North Carolina
2011

Approved by:

| | |
|---|---|
| _____ | _____ |
| Dr. Zerihun Assefa<br>Major Professor | Dr. Alex Williamson<br>Committee Member |
| _____ | _____ |
| Dr. William Adeniyi<br>Committee Member | Dr. Margaret Kanipes-Spinks<br>Department Chairperson |

_____
Dr. Sanjiv Sarin
Associate Vice Chancellor for Research and Graduate Dean

# Dedication

This thesis is dedicated to Jala, Jalanté, and Tyanna Whitehead.

# Biographical Sketch

Kendra Evette Whitehead was born October 19, 1982, in Dunn, North Carolina. She obtained her high school education at Triton High School in Erwin, North Carolina in 2000. She received the Associates of Science degree in Computer Programming from Guilford Technical Community College in 2003. She received the Bachelor of Science degree in Chemistry from North Carolina Agricultural & Technical State University in 2005. She is a candidate for the M.S. in Chemistry.

Acknowledgements

I would like to thank God who gave me the strength and perseverance to continue when I wanted to give up. I would like to express my heartfelt gratitude to my major advisor Dr. Zerihun Assefa for his sincere and selfless support during my research. Special thanks are given to my thesis advisory committee members Dr. Alex Williamson and Dr. William Adeniyi. I would like to give special thanks and say I love you to my father and mother – Johnnie and Brenda Whitehead, my sisters, my brothers, and my close friends – Junia Selby, Darkus Jenkins, Matthew Mickens, and Carlos Crawford for their infinite support. Thank you, Ms. Carolyn Mayo, for your wisdom and guidance. Thank you, Mr. King, for your instrumentation help. I would especially like to thank the loves of my life, my children - Jala, Jalanté, and Tyanna. Thank you for the hot cocoa, Wii breaks, silly dances and songs, the decorative artwork on my important papers, pitta patta of feet all through the house, and for reminding me of my purpose in life. Mommy did it all for you! Thank you Tyrus Davis for the nights spent listening about 1,3,5-triaza-7-phosphaadamantane-7-oxide complexes, smile I love you. I would also like to thank my family and friends for their encouraging words. Thank you to the Department of Chemistry, faculty, staff, and students. This project was supported by the National Oceanic and Atmospheric Administration Education Partnership Program award number NA06OAR4810187.

Table of Contents

List of Figures

List of Tables

# List of Symbols

| | |
|---|---|
| Å | Angstrom |
| EtOH | Ethanol |
| g | Gram |
| MeOH | Methanol |
| Me | Methyl |
| mL | Milliliter |
| TPA | 1, 3, 5-triaza-7-phosphaadamantane |
| TPAO | 1, 3, 5-triaza-7-phosphaadamantane-7-oxide |
| $PH_3$ | Phosphine |
| PLD | Phospholipase |
| UV | Ultraviolet |
| Ln | Lanthanide |
| PTI | Photon Technology International |
| IR | Infrared Spectroscopy |
| nm | Nanometer |
| Terpy | Terpyridine |

# Abstract

This work presents basic research in the area of lanthanide spectroscopy that could have the potential in chemical sensor technology. As part of the overall theme of developing synthetic scheme that may remove water from lanthanide inner sphere coordination we have targeted phosphines oxides. The synthesis of lanthanide TPAO compounds have been carried out by a reaction of $Ln^{3+}$ trichloride hexahydrate and TPAO in solvent system containing water. The TPA system was particularly targeted because of its unique property of having a small cone angle (102°) and water solubility and stability. We have attempted to coordinate up to four TPAO into the Eu inner sphere. We were able to characterize crystallographically the structural features of the bis-TPAO complex. The distorted square antiprism $[Eu(TPAO)_2(H_2O)_6]Cl_3$ has been structurally characterized. The compound crystallizes in the orthorhombic crystal system and the space group is, Pccn. Unit cell parameters are a = 35.992(5) Å, b = 10.0915(14) Å, c = 16.638(2) Å, $\alpha = \beta = \gamma = 90^{\circ}$. In addition, in our attempt to develop dual donor system for lanthanide sensitization we have structurally characterized a terbium system consisting of a terpy ligand and a group 11 transition metal complex coordinated simultaneously to a Tb system. The structural feature of the complex shows a distorted antiprismatic $Tb(Au(CN)_2)_3(Terpy)\cdot 4H_2O$ geometry. This complex crystallized in a triclinic system and the space group is, P 1 21/n1 with unit cell parameter of a = 10.6419(17), b = 16.407(3), and c = 24.992(4) Å with $\alpha = 90^{\circ}$, $\beta = 98.535(5)^{\circ}$, and $\gamma = 90^{\circ}$. The studied phosphine oxide and terpy has strong absorbance corresponding to n-$\pi^*$transition and may act as light harvesting antennae and can subsequently transfer absorbed energy to coordinated Ln(III) cations. Detailed spectral and crystallographic discussions of the compounds are reported in this thesis.

# CHAPTER 1

## Introduction

### 1.1 Luminescence

The history of luminescence can be traced back to the beginning of written history. However, the scientific explanation was reported in 1888 by the German Physicist Eilhardt Wiedemann [1]. Luminescence can be defined as emission of light energy input into a system. There are many ways that this can occur including absorption of light, chemical reaction, bio-chemical reactions, mechanical, or thermal energy exchanges. In the process of luminescence electrons are excited and promoted to a higher energy level. When electrons return to the ground state from an excited state, quanta of light is emitted.

The primitive roots of luminescence stemmed from the aurora borealis, luminous animals (fireflies, glow worms), phosphorescent wood, or stones (Bolognian stone) [2]. Various types of luminescence exist such as bioluminescence, chemiluminescence, triboluminescence, and photoluminescence to name a few. Bioluminescence is created when a living organism emits light through a chemical reaction such as fireflies, krill, and comb jellies. Chemiluminescence refers to the emission of light due to the release of energy from a chemical reaction. Examples of chemiluminescence can be seen by the use of glow sticks and luminol (when mixed with an appropriate oxidizing agent).

Triboluminescence involves generating light through the scratching, crushing, or rubbing of material in effort to break a chemical bond such as in a diamond or sucrose sugar. In photoluminescence a complex absorbs photons in which the photons are then excited to a higher energy state and emit a photon upon returning to a lower energy state. In the ultraviolet region of the electromagnetic spectrum is typically were these photons are absorbed and then output in the

visible region of the spectrum. Photoluminescence can be classified into two subcategories, fluorescence or phosphorescence.

Fluorescence is an optical occurrence that presents itself as glowing light. Due to the minimal heat emitted by most fluorescent substances it is referred to as cold light. In fluorescence, photons are absorbed in the ultraviolet region of the spectrum and the excess energy is liberated from an excited state of the same multiplicity as the ground state. Multiplicity is defined as 2S+1, where S represents the angular spin momentum [3]. It differentiates several degenerate wavelengths that vary merely in the orientation their angular spin momentum. The transition for fluorescence is classified as spin allowed.

Phosphorescence is the ability of a substance to emit light after it has been expose to and removed from the initial activating ultraviolet light. This radiative [4] decay takes place from a state of multiplicity different from that of the ground state [5]. This process is spin-forbidden therefore intersystem crossing becomes of importance for the reason that the initial excitation of a phosphorescent compound normally populates a spin allowed transition. Intersystem crossing is the nonradiative tradition of the first excited state into another excited state of different multiplicity. Lifetimes for these transitions range from milliseconds to minutes.

Luminescent material referred to as phosphors are rare earth metal or transition metal compounds that exhibit luminating properties. Phosphors are compounds capable of converting short wavelength radiation into longer wavelengths [6]. These phosphors typically consist of a host structure into which activator ion are introduced. Activator ions have the ability to absorb and emit light of desired wavelengths. Dressler and coworkers [7] discussed probing the utilization of rare earth metal ions as fluorescent markers for the enzyme phospholipase (PLD). They discovered the lanthanide $Tb^{3+}$ bound to PLD with an increase in the signal. In comparison

to the $Fe^{3+}$ ions it was found that lanthanides are efficient probes for analyzing the role of metal ions in PLD regulation. The activator ions are certain lanthanide ions or d-metals, such as $Ag^{+}$, $Mn^{+2}$, and $Eu^{2+}$ [5]. Luminescent materials are used is various application like television screens, medical scanners, brake lights, etc. Many combinations of these materials have been examined with the intent of efficiently converting ultraviolet (UV) radiation into a desired emission color.

**1.2 Lanthanides and Their Chemistry**

Lanthanides are referred to as lanthanoids in many publications due to the fact that the suffix -ide signifies that the element is negatively charged as in chloride ($Cl^{-}$), bromide ($Br^{-}$), etc. They are commonly classified as rare earth elements although they are not as rare as originally thought. Lanthanides are generally represented by the symbol Ln. Atomic numbers 58-71 makeup the lanthanide series in the periodic table [8]. They are silvery-white and shiny metals that oxidize easily when exposed to air. These soft metals increase in hardness with the atomic number. The lanthanides possess similar chemical properties to those of electropositive metals. They are comparatively poor conductors of heat and electricity. The lanthanide series are characterized by the consecutive filling of the 4f orbitals.

The most common oxidation form of lanthanides occur as Ln (III); due to the fact the f electrons are detained by the nucleus once the s and d electrons have been removed [5]. The electrons in the 4f shell and their trivalent ions are shielded by the outer $5s^2 5p^6$ subshell of the xenon arrangement. The 4f orbitals go through the xenon core significantly which enables them from overlapping with ligand orbital, for that reason $Ln^{+3}$ ions do not take part in bonding [2, 4, 8]. Due to the protected 4f orbitals the influence generated by counter anion molecules or ligands are very minimal [8]. $Ln^{+3}$ ions are hard Lewis acids which prefer oxygen containing ligands and occur in $PO_4^{3-}$ minerals.

Lanthanide complexes have received great attention due to appealing luminescence properties and a wide range of applications. All lanthanides with the exception of $Lu^{3+}$ exhibit luminescence abilities. $Eu^{3+}$ and $Tb^{3+}$ have very strong emissions attributable to the number of excited states which increases the probability of intersystem crossing and population of excited states of different spin multiplicity from the ground state [5, 9]. The majority of lanthanide ions are feebly colored although has sharp absorption spectra. The f-electrons transitions are accountable for the photophysical properties of the lanthanide ions long-lived luminescence and sharp absorption and emissions lines. Specifically, lanthanide ions present sharp characteristic emission in the visible and near-infrared (NIR) ranges, long luminescence lifetimes, and large Stokes shifts, which makes them very attractive candidates for the development of optical devices. Ligands that contain strongly absorbing chromophores can be conveniently used to sensitize lanthanide emission at low energy [10].

**1.2.1 Europium and Spectroscopic Studies.** The element europium has an electron configuration of [Xe] $4f^7 6s^2$. It is the most reactive of all the lanthanides and has the lowest melting point 822°C [11]. Monazite and bastnasite are the most common ores where europium can be found. Europium is very difficult to isolate from the ore. Rabie and coworkers [12] discussed the efficient separation of europium using a two step process. Reduction was employed first utilizing a zinc column and secondly precipitation using sulphate salt under inert atmosphere. They were able to obtain a europium yield of 91% with a purity of 97%.

Europium is a ductile metal that rapidly oxidizes in air. Its oxidation state varies from +2 and +3 (which is most common). Eu exists as a trivalent ion with and electronic configuration of $4f^6$. The coordination number for a trivalent europium ion complex is generally eight or nine. Europium (III) complexes have been investigated for a number of reasons. They are known to

have uses for lighting devices, computer and television displays, sensors [13], solid state lasers [14], luminescent probes in biomolecular systems [4, 15], and to have photochemical and photophysical properties. The excitation spectra $^7F_0 \rightarrow {}^5D_0$ transition of the Eu (III) ion has shown to be a predominantly valuable feature. A singlet peak in the excitation spectrum is observed in the Eu (III) enviroment due to the ground and excited states being non-degenerate. The forbidden transition of the 0-0 band are extremely weak. The symmetry selection rules prohibts the 0-0 transition when the Eu (III) ion is in a high symmetry or center of inversion enviroment [8]. The UV absorption spectra of europium complexes have an intense absorption mostly in the range of 200 - 400 nm and have an orange emission spectra between 580 -620 nm [16].

Wegh and coworkers [17] have been investigating ways to replace mercury discharge by noble gas discharge in fluorescent tubes. They demonstrated the quantum cutting. In their studies a two-step energy transfer from $^6G_J$ levels of $Gd^{3+}$ to two $Eu^{3+}$ ions in $LiGdF_4:Eu^{3+}$ and $GdF_3:Eu^{3+}$ was conducted. The concept offers the possibility of a phosphor with visible quantum efficiency close to 200%.

**1.2.2 Terbium and Spectroscopic Studies.** Terbium a member on the lanthanide series denoted by the molecular symbol Tb and atomic number 65 occupies period 6 of the periodic table. It is a silvery white metal that is malleable, ductile, and comparatively stable in air. Terbium can easily oxidize. Its oxidation states vary from +3 and +4. It mostly exhibits the oxidation state of +3. Terbium is not found in nature as a free element; it is contained in many minerals such as cerite, gadolinite, and monazite to name a few [18]. Compounds containing terbium should be handled with care due to the low to moderate acute toxic rating.

The electron configuration of terbium is [Xe] $4f^9 6s^2$. Terbium ions ($Tb^{3+}$) have a ground configuration of [Xe] $4f^8$. With the 4f shell being unfilled the electrons in the 4f shell are optically active. The principal quantum number determines the average distance of the shell from the nucleus therefore leaving the filled 5s and 5p shells to shield the optically active 4f electrons. Long fluorescence lifetimes and narrow spectral lines are produced in the shielding process. The Dieke diagram can be utilized to display the possible energy level transition for terbium (see Figure 1.1).

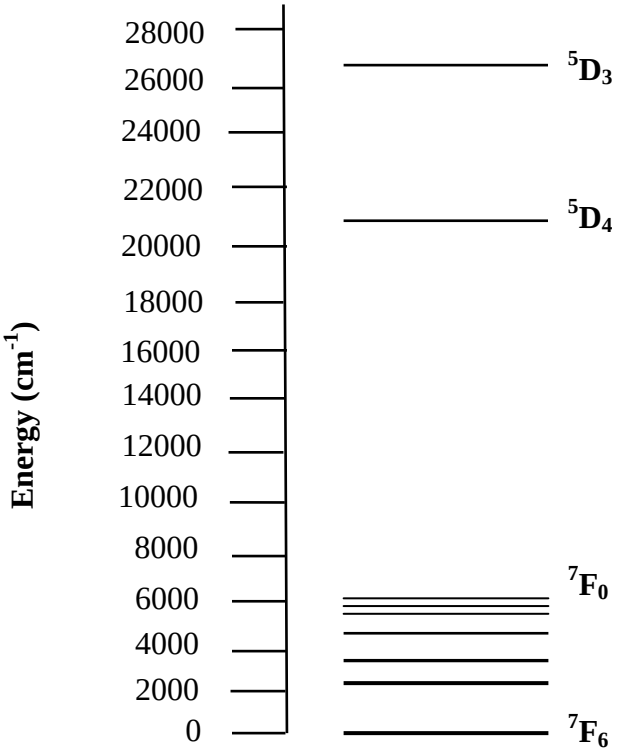


*Figure 1.1.* The Dieke diagram energy Levels of $Tb^{3+}$ [19].

Terbium (III) complexes have strong fluorescent abilities which result in a strong green emission when examined. Terbium radiates a luminous green color when in the correct wavelength. A rich emission spectrum in the 400 nm to 460 nm range is observed when $Tb^{3+}$ ions are excited to the $^5D_3$ level, decaying to different $^7F_J$ ground state levels. The most intense

transitions of $Tb^{3+}$ ion is the energy level $^5D_4 \rightarrow {}^7F_5$, which corresponds to a green emission band near 546 nm [20]. Terbium is utilized in luminescent probes and stains, [15] its oxide in green phosphors, [21] to dope calcium fluoride and other chemicals in solid state devices, and as a crystal stabilizer in fuel cells [22].

### 1.3 Ligands

Ligands are ions or molecules that coordinate to a central metal atom to form coordination complexes. It can have an independent existence. Ligands act as Lewis bases, and electron donor, and the metal acts as a Lewis acid, and electron acceptor. These acids and bases can be classified as hard or soft acids and bases, as well as according to their polarizability The degree of distortion by the interactions of molecules or ions with other molecules can be use to understand acids and bases. The area of inorganic chemistry is where a central metal ion or atom complexes or coordinates with one or more molecules that surround the central species is known as coordination chemistry.

Ligands play a key role in coordination chemistry. Normally ligands are bound to metals by donating electrons from a lone electron pair to a metal with an empty orbital. They can have single pair of donor electrons which means that have one point of attachment to the metal and are referred to as monodentate. Ligands that contain two points of attachment are bidentate and those with more than one point of attachment are known as polydentate.

**1.3.1 Tertiary Phosphine Oxides as Ligands.** Phosphine oxides are organophosphorus compounds with the formula ($O=PR_3$) where R could represent an alkyl, aryl, or hydrogen. They are the most common auxiliary ligands used in organometallic chemistry. The general formula for phosphine is $PR_3$. Tertiary phosphines exist in various derivations with $PH_3$ being the simplest. Phosphine ($PH_3$) is the parent compound of phosphines, which is a reactive, flammable,

colorless, poisonous gas. Organophosphines are soft ligands which are frequently incorporated into metal complexes with the central metal atom in low oxidation states [5]. Organophosphines have the ability to stabilize low metal oxidation states and they can be easily modified. Tertiary phosphines have distinct σ-donor and π-acceptor abilities and resistance to chemical transformation which is of great importance [23]. When discussing the reactivity of phosphine complexes two properties are considered important; their electron donating ability and steric bulk [5].

Tolman [24] classified phosphorus ligands according to their steric size utilizing a geometrical parameter system, known as cone angle. Bulky ligands have larger cone angle. Selected Tolman cone angles values for phosphine ligands are shown in Table 1.1. The steric parameter Θ for $PR_3$ defined by Tolman is the apex angle of a cylindrical cone which is centered at 2.28 Å from the center of the P-atom, which touches the van der Waals radii of the outermost atoms of the model.

Table 1.1

*Selected Cone Angles*

| **Ligand** | **Cone Angle °, deg** |
|---|---|
| $PH_3$ | 87° |
| TPA | 102° |
| $PF_3$ | 104° |
| $P(OMe)_3$ | 107° |
| $PMe_3$ | 118° |
| $PCl_3$ | 125° |
| TFP | 133° |
| $PPh_3$ | 145° |

The tertiary phosphine that has been investigated in this research is 1, 3, 5-triaza-7-phosphaadamantane (TPA). The water soluble cage-like aminophosphine ligand consists of an adamantane group with three nitrogen atoms and one bridgehead phosphorous atom. The multifunctional ligand with a cone angle of 102° has gained attention. The monodentate ligand was first reported by Daigle et al. in the 1970s. Initially it was proposed to create flame proof polymers [25]. An inert atmosphere is not a requirement for the synthesis of TPA. It is neither air nor moisture sensitive. TPA is thermally stable and decomposes at temperatures higher than 260° [25]. One distinctive characteristic of TPA is the ability to be regioselectively protonated at nitrogen versus the phosphorous center. Coordination of a single metal through P, N or N, N atoms pose a problem due to the geometric constraints. The TPA ligand can act as bridging ligand between two or more metal centers. The aminophosphine ligand can bind up to four Lewis acids attributable to the four potential coordination sites [26].

Frost and coworkers [27] were able to coordinate a series of group 12 metal complexes such as $Zn^{2+}$, $Cd^{2+}$, and $Hg^{2+}$ with TPA derivatives. The rarely observed nitrogen bound TPA coordination modes diversify its chemistry, building up coordination polymers and multinuclear metal complexes. Wong and coworkers [28] have made the first modification to the upper rim of the TPA ligand. The lithiation of TPA deprotonated the α- phosphorous methylene yielding the formation of TPA-Li. Utilizing the TPA-Li, Wong et al. synthesized a new chiral chelating phosphine TPA-$PPh_2$. Huang and coworkers [29] utilized the $P(CH_2NH_2)_3$ as the initial trisubstituted triazaphosphaadamantane ligand. The lower rim of the TPA derivatives were trisubstituted in the synthesis of cyclocondensation of varying aldehydes with tris(aminomethyl)-phosphine. Modifying the ring of the TPA allowed the altering of sterics of the phosphine while keeping changes to the electronics very minimal.

The basicity of the neighboring nitrogens decreases when the phosphorous center is oxidized. TPA can be oxidized by photo-oxidation by light as well as by treatment with hydrogen peroxide, a strong oxidizing agent. In this study 1, 3, 5-triaza-7-phosphaadamantane (TPA) was oxidized using hydrogen peroxide forming 1, 3, 5-triaza-7-phosphaadamantane-7-oxide (TPAO).

**1.3.2 Terpyridine as a Ligand.** The molecule terpyridine is a polypyridine compound consisting of three nitrogen atoms and therefore it can act as a tridentate ligand. 2,2":6,2"-terpyridine (terpy) forms stable chelates with several metal ions. Terpy possess attractive features for the construction of tunable chromophores with its affinity for cations [30]. The terpy ligand are coordinated to lanthanides in which the ligand absorbs exciting near UV radiations and channels it to the lanthanide ion [31]. Metal complexes of terpy have been utilized in various applications, photosensitizers for solar energy, and supramolecular assemblies and DNA metallointercalators [32].

The terpy ligand is used in photonic applications due to the interest in optical properties of sol-gel derived siloxane hybrid materials containing luminescent species. The covalent attaching of the terpy ligand to a silica backbone via Si-C bonds was studied by Tong et al [31]. The compound terpy-Si was synthesized by thiol-ene photopolymerization. Terpy-Si has two roles; it serves as a ligand to the lanthanide ions and as a precursor for the sol-gel process. The techniques of hydrolysis and co-condensation of tetraethoxysilane and terpy-Si in the presence of $Eu^{3+}$ or $Tb^{3+}$ were employed in preparing the luminescent hybrid materials. Strong emissions of $Eu^{3+}$ and $Tb^{3+}$ ions via intramolecular energy transfer for the triplet energy state of the terpy to the resonant emissive level of the lanthanide ions were shown, therefore, making it useful in electronic and optical applications [31].

Terpy ligand is seen in the search process of proactive ligands for $Eu^{3+}$ and $Tb^{3+}$ ions. The development of lanthanide luminescence spectroscopy for in vitro and in vivo biomedical diagnostics impelled the search [33]. Galaup et al. planned the groundwork of the triaza-triacetate ligand containing a terpy component as part of its macrocyclic ring. The terpy group is appropriate for energy absorbing and transferring component. It displays an intense absorption band in the near UV region. The carboxylic acid groups permit the formation of strong neutral complexes due to the establishment of electrostatic interactions and increased solubility in water solutions [34]. The lanthanide proactive ligand can be utilized as luminescent biolabels.

**1.3.3 Gold (I) Dicyanide.** Dicyanoaurate (I) ions have proven to be good candidates as donors in energy transfer studies. Dicyanoaurate (I) ions are tunable and display a red shift with increasing concentration or decreasing temperature [35]. Guo et al. reported tunable energy transfer between $d^{10}$ metal dicyanide nanocluster donor ions and $Eu^{3+}$ and $Tb^{3+}$ acceptor ions in nonaqueous solvents. Methanol, acetonitrile, and dioxane were used as solvents. In this study concentration, excitation wavelength, and solvents were varied to examine the tunability of the emission energy of $d^{10}$ metal dicyanide nanocluster ions [36].

Assefa et al. [37] studied the photoluminescence of lanthanide ion complexes of metal dicyanides. The structure of the compounds consist of linear $Au(CN)_2^-$ ions layered alternating with $M^{n+}$ ion layers. The excited state energy transfer process is observed in the low dimensional complexes which are layered.

The $Eu^{3+}$ ion has proven to be unique in the ability of having a ground state $^7F_0$ and emissive state $^5D_0$ to be nondegenerate. The energy transfer process in $Eu[Au(CN)_2]_3$ and $Eu[Ag(CN)_2]_3$ compounds were investigated [37]. The Au-Au covalent interactions were greater

than the Ag-Ag covalent interactions. The $Eu[Au(CN)_2]_3$ system displayed low lying charge transfer while occupying two lattice sites [37].

The purpose of this investigation is to develop techniques such as sensitization, in the event to elude the Laporte forbidden inefficient f-f transitions. One well-known problem in lanthanide spectroscopy is the existence of $H_2O$ in the inner sphere coordination. Modification of phosphine ligands are considered to play a dual role in the replacement of the quencher $H_2O$ and serve as effective sensitizer. Development of multiple donor systems in which can be excited concurrently for cooperative sensitization is another objective of this research project. A complex consisting of a terpy ligand and a group 11 transition metal complex coordinated simultaneously to a terbium system is expected. The studied phosphine oxide and terpy containing complexes have strong absorbance corresponding to n-$\pi^*$ transition and may act as light harvesting antennae and can subsequently transfer absorbed energy to coordinated Ln(III) cations. We have characterized these complexes using a variety of spectroscopic techniques including X-ray crystallography, infrared spectroscopy (IR), and luminescence spectroscopy.

# CHAPTER 2

## Experimental Methods

### 2.1 Chemical Reagents

The chemicals used in this study for synthesis, recrystallization, and spectrochemical analysis are acetonitrile, ethanol, methanol, hydrogen peroxide, $EuCl_3 \bullet 6H_2O$, $TbCl_3 \bullet 6H_2O$, TPA, TPAO, $KAu(CN)_2$, and Terpy. They were used as purchased without further purification.

### 2.2 Syntheses

**2.2.1 Synthesis of TPAO. S**ynthesis of TPAO was conducted using 0.5g, ($3.2 \times 10^{-3}$mol) of TPA dissolved in 20 mL of methanol. A solution consisting of 0.5 mL 30% $H_2O_2$ in 20 mL of ethanol was slowly added to the solution of TPA using a Pasteur pipette. The resulting solution, which contained a small amount of white precipitate, was stirred for 20 minutes. The solvent was allowed to evaporate under a hood at room temperature until complete dryness. The product was recrystallized using hot ethanol.

**2.2.2 Synthesis of $[Eu(TPAO)_2(H_2O)_6]Cl_3$.** Synthesis of $[Eu(TPAO)_2(H_2O)_6]Cl_3$ was carried out using 0.050g of $EuCl_3 \cdot 6H_2O$ and 0.050g of TPAO. The metal and ligand was placed in a 20 mL beaker and 2 mL of distilled $H_2O$ was added. The solution was stirred for 15 minutes, covered slightly with parafilm, and placed on counter for slow evaporation at room temperature.

**2.2.3 Synthesis of $[Eu(TPAO)_4(H_2O)_4]Cl_3$.** Synthesis of $[Eu(TPAO)_4(H_2O)_4]Cl_3$ was conducted by dissolving 0.052g of $EuCl_3 \cdot 6H_2O$ in 3 mL EtOH in a test tube. The solution was heated and stirred for 5 minutes. In a separate test tube 0.096g TPAO was dissolved in 2 mL MeOH. The TPAO solution was mixed for 5 minutes and slowly pipette into the test tube containing the $EuCl_3 \cdot 6H_2O$ mixture. The tube was covered slightly with parafilm for slow evaporation in the hood at room temperature.

**2.2.4 Synthesis of $[Tb(TPAO)_2(H_2O)_6]Cl_3$.** Synthesis of $Tb(TPAO)_2(H_2O)_6]Cl_3$ was performed by placing 0.051g $TbCl_3 \cdot 6H_2O$ in a 20 mL beaker. A 0.048 g of TPAO along with 5 mL of distilled $H_2O$ was added to the beaker. The solution was stirred for 20 minutes. The beaker was covered slightly with parafilm and placed under the hood for slow evaporation.

**2.2.5 Synthesis of $[Tb(TPAO)_4(H_2O)_4]Cl_3$.** The synthesis of $[Tb(TPAO)_4(H_2O)_4]Cl_3$ was conducted by dissolving 0.098g of TPAO in 2 mL of MeOH and 2 mL of distilled $H_2O$ in a 20 mL beaker. The solution was heated and stirred for 5 minutes. A second 20 mL beaker contained 0.056g $TbCl_3 \cdot 6H_2O$ and 3 mL of EtOH was heated and stirred for 5 minutes. The TPAO solution was added to the beaker containing the $TbCl_3$ solution and heated and stirred for 10 minutes. The beaker was covered with parafilm and placed under the hood for slow evaporation.

**2.2.6 Synthesis of $Tb(Au(CN)_2)_3(Terpy) \cdot 4H_2O$.** The synthesis of $Tb(Au(CN)_2)_3(Terpy) \cdot 4H_2O$ was conducted using 0.107g $TbCl_3 \bullet 6H_2O$, 0.078g of $KAu(CN)_2$, 0.131g of TPAO was placed in a 50 mL beaker along with 5mL of distilled $H_2O$ and 3mL of MeOH. In a second beaker (20mL), 0.0694g of $C_{15}N_3H_{11}$ was placed along with 2 mL of acetonitrile. The contents of both beakers were stirred for 15 minutes. The contents of the second beaker containing the terpy solution were added to beaker 1, along with 7 mL of acetonitrile. The mixture was stirred for 10 minutes. Beaker was covered with parafilm to allow slow evaporation at room temperature.

**2.3 Spectroscopic Methods**

Samples were analyzed using spectrometric techniques that included vibrational and luminescence instruments. The IR spectra were collected using IR Prestige 21 Shimadzu FT-IR spectrophotometer. Steady-state emission and excitation were collected on a Photon Technology

(PTI) photomultipler Detection System.

**2.4 X-ray Crystallography**

X-ray intensity data was collected on a SMART X2S diffractometer using Mo-$K_\alpha$ radiation. The images were interpreted and integrated with the program AXS from Bruker. The structure was solved and refined using the Bruker SHELXTL Software Package, using the space group P 1 21/n 1, with Z = 4 for the formula unit, $C_{36}H_{36}Au_3N_{12}O_7Tb$. The final anisotropic full-matrix least-squares refinement on $F^2$ with 534 variables converged at R1 = 7.26%, for the observed data and wR2 = 18.96% for all data. The goodness-of-fit was 0.963. The largest peak in the final difference electron density synthesis was 1.890 $e^-/Å^3$ and the largest hole was -1.965 $e^-/Å^3$ with an RMS deviation of 0.321 $e^-/Å^3$. On the basis of the final model, the calculated density was 2.307 $g/cm^3$ and F(000), 2776 $e^-$.

**2.5 Photoluminescence Measurements**

The luminescence spectra were collected using a photon technology international (PTI) spectrometer (model QM-7/SE). The system uses a high intensity xenon source for excitation. Selection of excitation and emission wavelengths are conducted by means of computer controlled autocalibrated “QuadraScopic” monochromators and are equipped with aberration corrected emission and excitation optics. Signal detection is accomplished with a PMT detector (model 928 tube) that can work either in analog or digital (photon counting) modes. All of the emission spectra presented are corrected to compensate for wavelength dependent variation in the system on the emission channel. The emission correction files which were generated by comparison of the emission channel response to the spectrum of NIST traceable tungsten light were used as received from Photon Technology International (PTI). The emission correction was conducted in real time using the PTI provided protocol. The instrument operation, data

collection, and handling were all controlled using the advanced FeliX32 fluorescence spectroscopic package. All of the spectroscopic experiments were conducted on neat crystalline samples held in sealed borosilicate capillary tubes. The low temperature measurements were conducted on samples inserted in a cold-finger Dewar flask filled with liquid nitrogen.

The samples were studied under liquid nitrogen atmosphere and room temperature. Qualitative comparisons of both temperatures were accomplished by conducting the experiment at liquid nitrogen in the cold-finger Dewar. Some room temperature data was collected after the evaporation of liquid nitrogen. The parameters were kept relatively the same for both temperatures. Excitation and emission are the two spectra that are normally taken during luminescence measurement. To obtain excitation, emission is held at a constant value while running the excitation and for emission the excitation is held constant.

# CHAPTER 3

## Results and Discussion

### 3.1 Infrared Spectroscopy of $[Eu(TPAO)_2(H_2O)_6]Cl_3$

The infrared spectroscopy (IR) data shown below in Figure 3.1 displays specific frequencies that are characteristic to the $[Eu(TPAO)_2(H_2O)_6]Cl_3$ complex. The IR spectra indicated the presence of $\nu_{OH}$ at 3220 $cm^{-1}$ and a $\nu_{CN}$ stretch at 1170 and 1150 $cm^{-1}$. The $sp^3$ hybridized $\nu_{CH}$ stretching is not seen below 3000 $cm^{-1}$ due to overlapping of the $\nu_{OH}$ stretching.

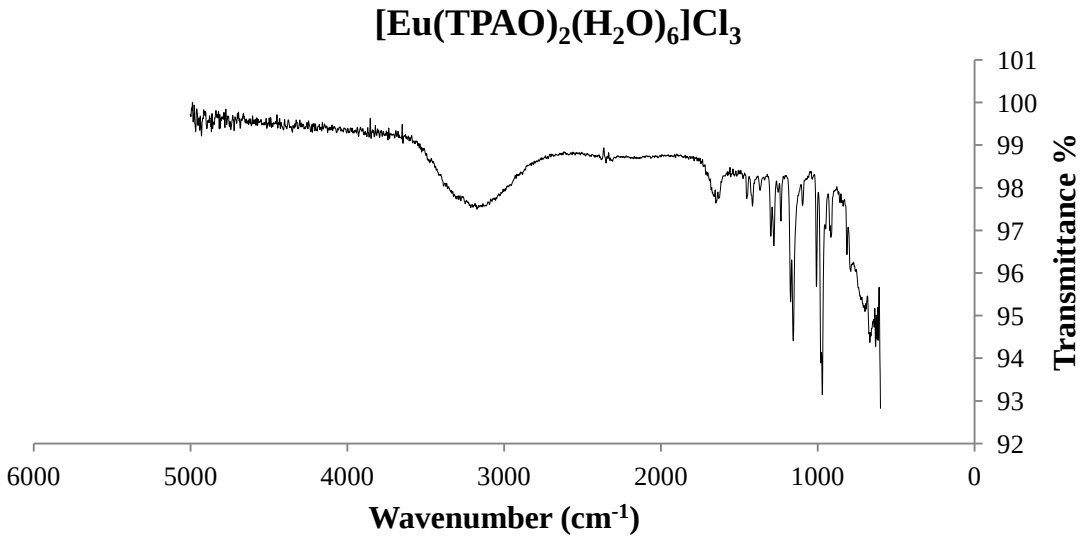


*Figure 3.1.* IR spectrum of $[Eu(TPAO)_2(H_2O)_6]Cl_3$

### 3.2 Crystal Structure of $[Eu(TPAO)_2(H_2O)_6]Cl_3$

The structure of $[Eu(TPAO)_2(H_2O)_6]Cl_3$ is shown in Figure 3.2. A crystal with dimensions of 0.50 x 0.50 x 1.00 $mm^3$ was used for x-ray analysis. The unit cell parameters are a = 35.992, b =10.0915, c = 16.638 Å with $\alpha = \beta = \gamma = 90^{\circ}$. The compound crystallizes in the orthorhombic crystal system and the space group Pccn. The $Eu^{3+}$ ion is coordinated to two TPAO ligands and six water molecules. The overall coordination environment of the Eu site is eight and has a geometry that is best described as distorted square antiprism. Additionally, three

uncoordinated water molecules are observed in the lattice. There are five uncoordinated chloride ions present in the lattice. The thermal ellipsoid of one chloride ion is larger due to thermal motion that exists in the lattice.

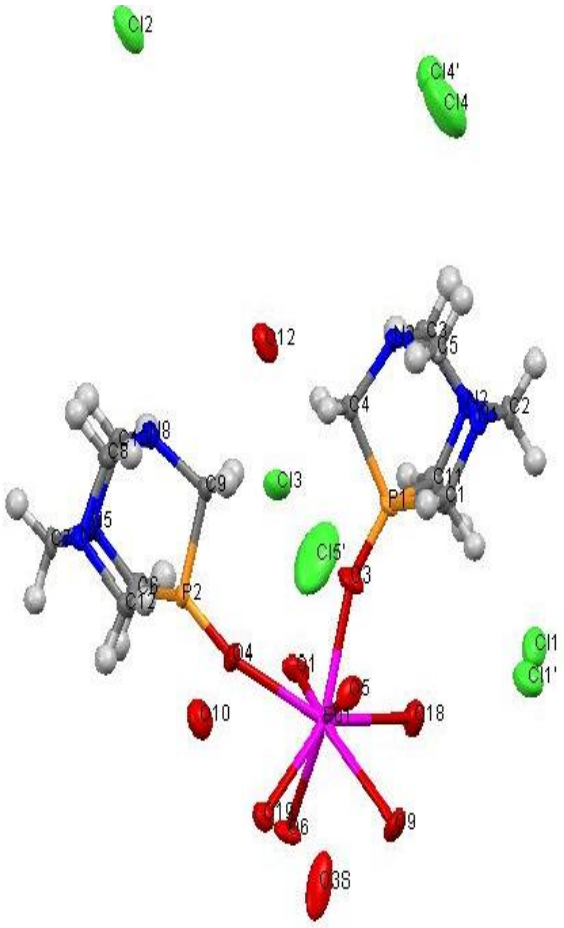


*Figure 3.2.* Crystal structure of $[Eu(TPAO)_2(H_2O)_6]Cl_3$ illustrating the coordination environment of the $Eu^{3+}$ site.

A summary of the crystallographic data are given Table 3.1. A detailed list of the bond distances and angles are given in Table 3.2. The two TPAO ligands coordinate through the oxygen atoms forming Eu-O bond distances of 2.331(3) and 2.366(3) Å. The six water molecules have an average Eu-O bond distance of 2.425 Å. The bond distance comparison indicates that on

average the Eu-O distance with the O atom of the TPAO is shorter by 0.07 Å than the bond distance with the $H_2O$ molecules. Stronger donor ability is inferred for the TPAO ligand, when compared with that of the $H_2O$ ligand.

Table 3.1

*Summary of the crystallographic data of $[Eu(TPAO)_2(H_2O)_6]Cl_3$.*

| | |
|---|---|
| Formula | $C_{13}H_{26}Cl_{3.75}EuN_6O_{13}P_2$ |
| Mol. Wt. | 821.24 |
| Dimensions ($mm^3$) | 0.50 x 0.50 x 1.00 |
| Crystal system | Orthorhombic |
| Space group | Pccn |
| a (Å) | 35.992(5) |
| b (Å) | 10.0915(14) |
| c (Å) | 16.638(2) |
| α (deg) | 90° |
| β (deg) | 90° |
| γ (deg) | 90° |
| Volume, $Å^3$ | 6043.1(14) |
| Temperature | 200(2) K |
| Z | 8 |
| Density (calculated) | 1.805 $Mg/cm^3$ |
| Absorption coefficient | 2.577 $mm^{-1}$ |
| Absorption correction | Multi-scan |
| F(000) | 3254 |
| Reflections collected | 52515 |
| Independent reflections | 5357 [R(int) = 0.0557] |
| Goodness-of-fit on $F^2$ | 1.148 |
| Final R indices [I>2σ(I)] | R1 = 0.0357, wR2 = 0.1039 |
| R indices (all data) | R1 = 0.0381, wR2 = 0.1057 |

$R_{int} = \Sigma| F_o^2 - F_o^2 (mean) | / \Sigma[F_o^2]$
$R_1 = \Sigma||F_o| - |F_c|| / \Sigma|F_o|$
$GOOF = S = \{\Sigma[w(F_o^2 - F_c^2)^2] / (n - p)\}^{1/2}$
$wR_2 = \{\Sigma[w(F_o^2 - F_c^2)^2] / \Sigma[w(F_o^2)^2]\}^{1/2}$
$w = 1 / [\sigma(F_o^2) + (aP)^2 + bP]$ where $P$ is $[2F_c^2 + Max(F_o^2, 0)] / 3$

Table 3.2

*Selected Bond Length (Å) and Angles (°) for $[Eu(TPAO)_2(H_2O)_6]Cl_3$.*

| | | | |
|---|---|---|---|
| Eu1-O4 | 2.331(3) | O4-Eu1-O3 | 77.85(12) |
| Eu1-O3 | 2.366(3) | O4-Eu1-O6 | 98.90(12) |
| Eu1-O6 | 2.375(3) | O3-Eu1-O6 | 146.65(11) |
| Eu1-O5 | 2.416(3) | O4-Eu1-O5 | 85.62(13) |
| Eu1-O1 | 2.435(3) | O3-Eu1-O5 | 74.19(12) |
| Eu1-O9 | 2.437(3) | O6-Eu1-O5 | 139.07(12) |
| Eu1-O18 | 2.442(3) | O4-Eu1-O1 | 79.17(13) |
| Eu1-O19 | 2.447(3) | O3-Eu1-O1 | 76.00(11) |
| | | O6-Eu1-O1 | 70.84(11) |
| | | O5-Eu1-O1 | 148.75(12) |
| | | O4-Eu1-O9 | 143.46(12) |
| | | O3-Eu1-O9 | 119.59(12) |
| | | O6-Eu1-O9 | 82.77(12) |
| | | O5-Eu1-O9 | 70.93(11) |
| | | O1-Eu1-O9 | 133.95(12) |
| | | O4-Eu1-O18 | 145.63(12) |
| | | O3-Eu1-O18 | 77.96(12) |
| | | O6-Eu1-O18 | 88.27(12) |
| | | O5-Eu1-O18 | 110.62(12) |
| | | O1-Eu1-O18 | 71.53(12) |
| | | O9-Eu1-O18 | 70.60(11) |
| | | O4-Eu1-O19 | 71.78(11) |
| | | O3-Eu1-O19 | 137.32(11) |
| | | O6-Eu1-O19 | 68.87(10) |
| | | O5-Eu1-O19 | 74.26(12) |
| | | O1-Eu1-O19 | 124.92(11) |
| | | O9-Eu1-O19 | 75.02(11) |
| | | O18-Eu1-O19 | 140.73(11) |

One of the goals of this project is to develop methods that would circumvent the Laporte forbidden inefficient f-f transition through the method of sensitization. The presence of coordinated water in the inner sphere coordination remains a prominent problem in lanthanide spectroscopy. An approach followed in this research is to rationally design systems that may induce complete removal of $H_2O$ from lanthanide inner sphere coordination. This removal of $H_2O$ has remained a challenge due to the high coordination number exhibited by these lanthanide ions. High $\nu_{OH}$ vibrational manifolds constitute an important nonradiative pathway that result in partial quenching of emissions from lanthanide ions. Carefully modified phosphine oxide ligands are thought to play a double role, as replacement of the quencher $H_2O$ and also as effective sensitizers.

The P=O group is known to form a strong bond with lanthanide ions through the oxygen atom [38]. Petrova, et al. [39] have used the coordinating power of phosphine oxides to separate lanthanum ions from aqueous solutions by liquid-liquid extraction. This work implies that P=O coordination can be used to block coordination of deactivating/luminescence quenching solvent molecules. By designing proper R groups in $R_xP=O$ moieties, it is possible to introduce a donor group that can transfer its excited energy to the metal center with high efficiency. In fact Iwanaga [40] was able to successfully coordinate two different phosphine oxides to a rare-earth ion and drastically enhance its emission intensity.

In collaborative work with the Sykora's group an interesting molecule was characterized recently, where up to four triphenylphosphine oxides were coordinated to lanthanide center as shown in Figure 3.3. Water was fully removed from the inner sphere coordination environment of the Tb system. The $Tb(Ph_3PO)_4(Au(CN)_2)_3$ complex displays three coordinated dicyanoaurate anions and four triphenylphosphine oxide molecules with no $H_2O$ in the inner sphere, although

the synthesis was conducted in aqueous media. This was rather unexpected since steric factors were thought to restrict the number of the $Ph_3PO$ ligands coordinating to the metal center.

The initial attempt in this work targeted the TPA ligand. As mentioned earlier, among the alkyl phosphines, TPA has two unique features. First it is highly soluble in water and stable. In addition, the multifunctional ligand has one of the smallest cone angles (102°) for any alkyl phosphine (Table1.1). It was thought that more TPA based phosphine oxides can coordinate to the metal center as needed. The initial step involved development of a mild oxidation technique to convert the phosphine to the respective phosphine oxide followed by lanthanide coordination. The coordination of the TPA ligand is thought to induce water solubility, but with no $H_2O$ molecule actually coordinated to the lanthanide inner sphere and, hence, emission enhancement is expected in aqueous media. Other phosphine ligands that were attempted include adducts of methyl-imidazole, benzimidazole, 2-(2-pyridyl)benzo[1,2-d;4,5-d'] diimidazole etc.

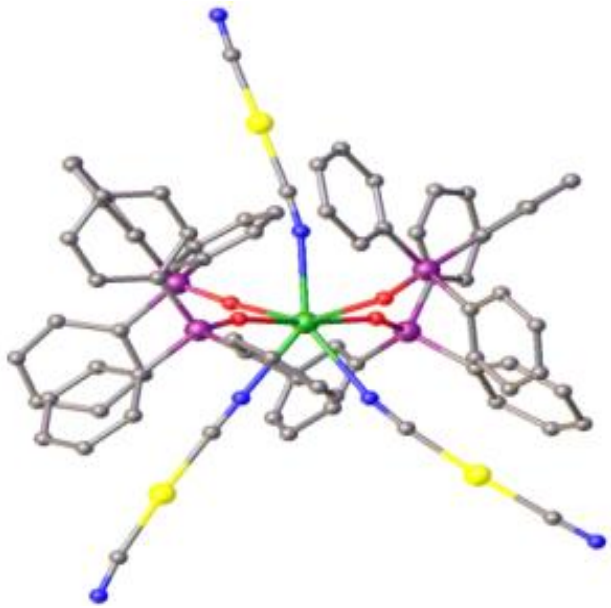

*Figure 3.3.* $Tb(Ph_3PO)_4(Au(CN)_2)_3$ complex. The compound was synthesized and its structure solved in Professor Sykora's group at the University of South Alabama [40].

Although a number of TPA complexes were attempted in this study only the bis coordinated complex was crystallized and structurally characterized, albeit with much difficulty due to large distortion in the lattice. The structural and photophysical studies are aimed at unraveling the details of the energy transfer mechanisms and the sensitization efficiency through temperature dependent, life-time, time-resolved, and luminescence studies as well as quantum yield investigations in rationally designed systems.

### 3.3 Infrared Spectroscopy of TPAO Ligand

The IR data shown below in Figure 3.4 displays specific frequencies that are characteristic of the TPAO ligand. The $\nu_{CN}$ stretch shows up at 1150 $cm^{-1}$. The $sp^3$ hybridized $\nu_{CH}$ stretching is observed at 2890 $cm^{-1}$.

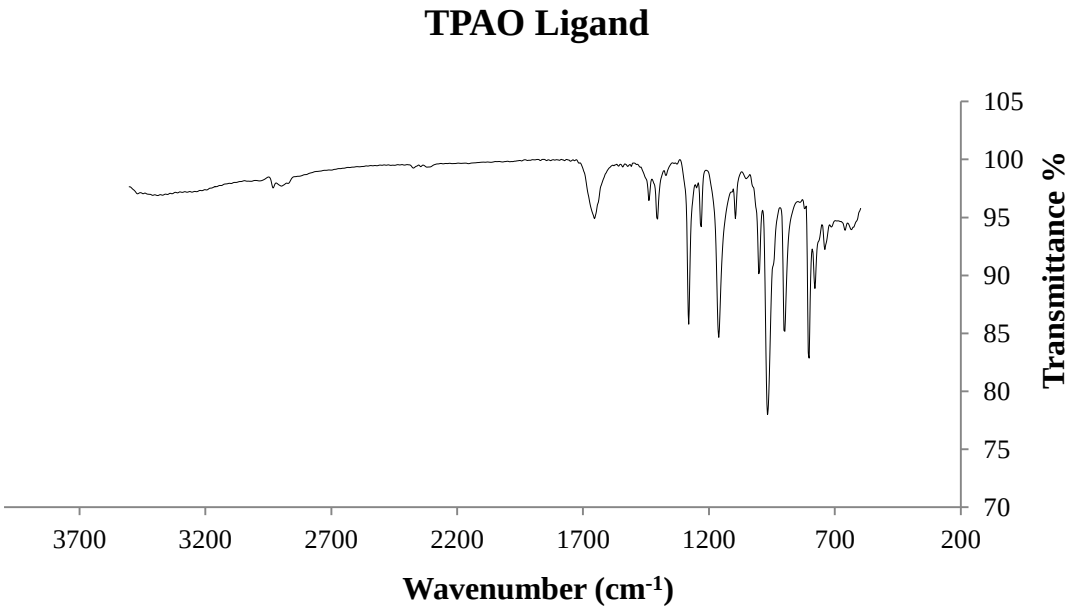


*Figure 3.4.* IR spectrum of TPAO

### 3.4 Photoluminescence Studies of TPAO Ligand

The excitation spectrum for the TPAO ligand shown in Figure 3.5a is collected in the 270 to 400 nm range, by monitoring the emission 426 nm. The water soluble aminophosphine oxide

at liquid nitrogen temperature displays an unsymmetrical broad emission band that maximizes at 426 nm. The organic ligand is expected to have a negligible influence on the 4f electrons of the lanthanide ions once coordinated.

A broad excitation band maximizes at 350 nm in the spectrum. Figure 3.5b is the emission profile of the TPAO is shown. The emission band maximizes at 426 nm when the sample was excited at 350 nm. The band is observed at an energy position shifted by 5100 $cm^{-1}$ when compared with the excitation maximum. This large shift indicates that the emission originates from the triplet ($^3\pi^*$) state.

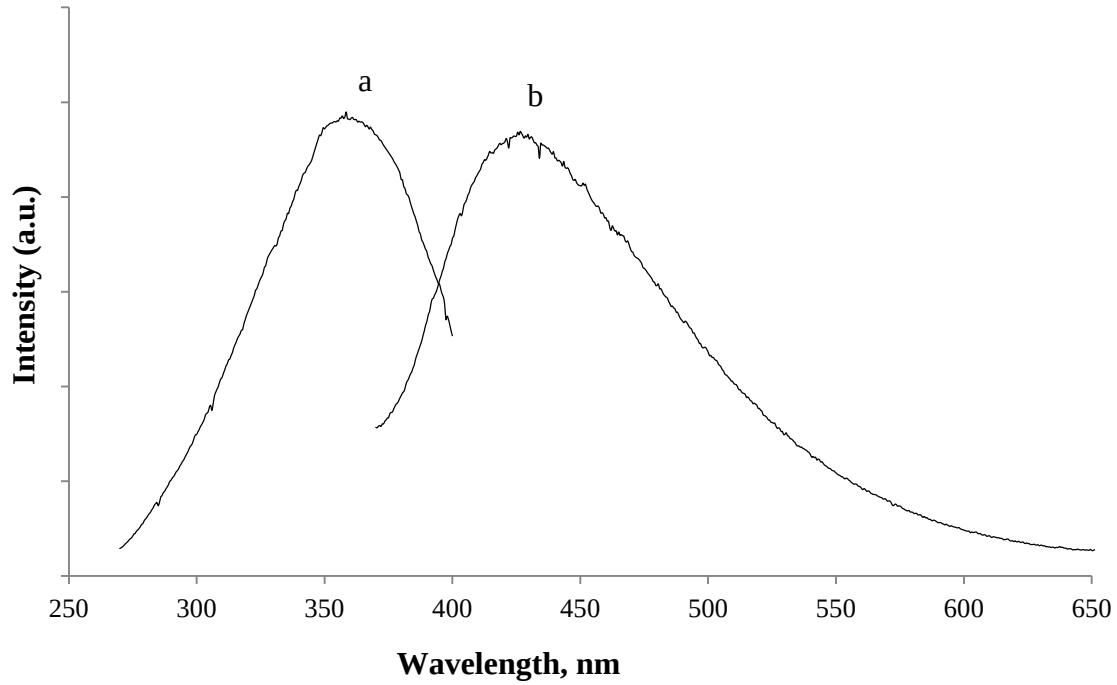


*Figure 3.5.* Excitation and emission spectra of TPAO ligand collected at liquid $N_2$ temperature: (a) Excitation monitored at 426 nm, (b) Emission excited at 350 nm.

### 3.5 Photoluminescence Studies of $[Eu(TPAO)_2(H_2O)_6]Cl_3$

The excitation spectra of $[Eu(TPAO)_2(H_2O)_6]Cl_3$ are shown in Figures 3.6. These spectra were collected at liquid $N_2$ while monitoring the emission at 592 and 612 nm for Figures a, and b

respectively. The most intense excitation band was observed around 382 nm which corresponds to the $^5L_6 \leftarrow {}^7F_0$ excited-state level. This band characteristic of f-f transition is sharp. However when collected at room temperature seen in Figure 3.7, the presence of more structural peaks appeared in the $^5G_2 \leftarrow {}^7F_0$ transition region.

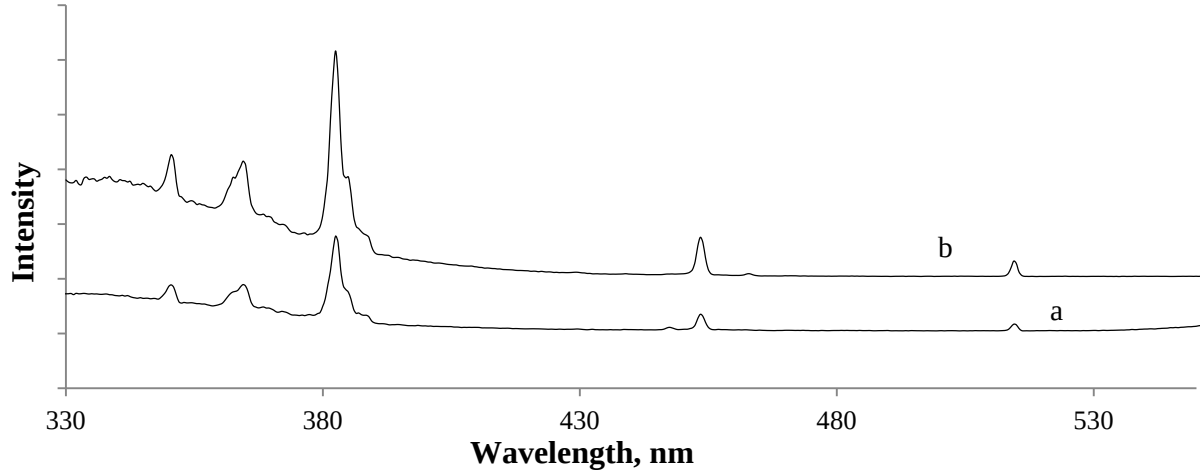


*Figure 3.6.* Excitation spectra of $[Eu(TPAO)_2(H_2O)_6]Cl_3$ collected at liquid $N_2$ temperature by monitoring the emission at: (a) 592, (b) 612 nm.

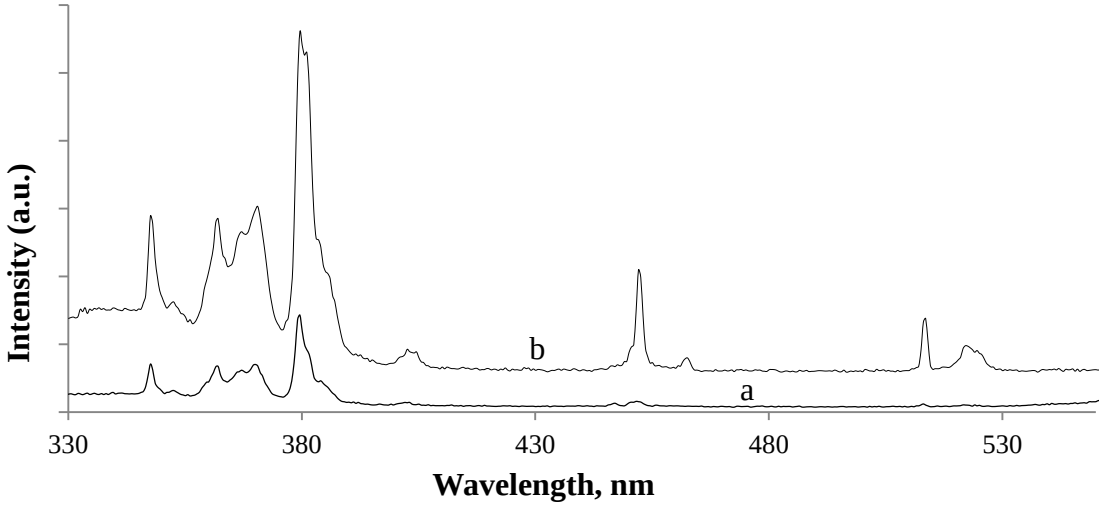


*Figure 3.7.* Excitation spectra of $[Eu(TPAO)_2(H_2O)_6]Cl_3$ collected at room temperature by monitoring the emission at: (a) 592, (b) 612 nm.

The emission spectra for $[Eu(TPAO)_2(H_2O)_6]Cl_3$ Figure 3.8 are recorded at liquid $N_2$ temperature. The emission spectra seen are in the range of 450 to 750 nm was excited at wavelengths of 364, 382, and 390 nm. An intense peak appears at 612 nm. The spectra consist of sharp emission lines characteristic of $Eu^{3+}$ f-f transitions. In Tables 3.3 and 3.4, the energies of $[Eu(TPAO)_2(H_2O)_6]Cl_3$ along with their assignments are given. Five peaks are observed over the $Eu^{3+}$ ion $^5D_0 \rightarrow {}^7F_0$, $^7F_1$ transition regions. The maximum number of splitting within the $^5D_0 \rightarrow {}^7F_1$, transition under low symmetry is 3. Two weak bands corresponding to the $^5D_0 \rightarrow {}^7F_0$ transition are shown. In theory, only a single band is expected in the $^5D_0 \rightarrow {}^7F_0$ for each type of $Eu^{3+}$ site. Since no splitting in the 0-0 transition is expected, regardless of symmetry, observance of two bands indicates the presence of two different europium sites.

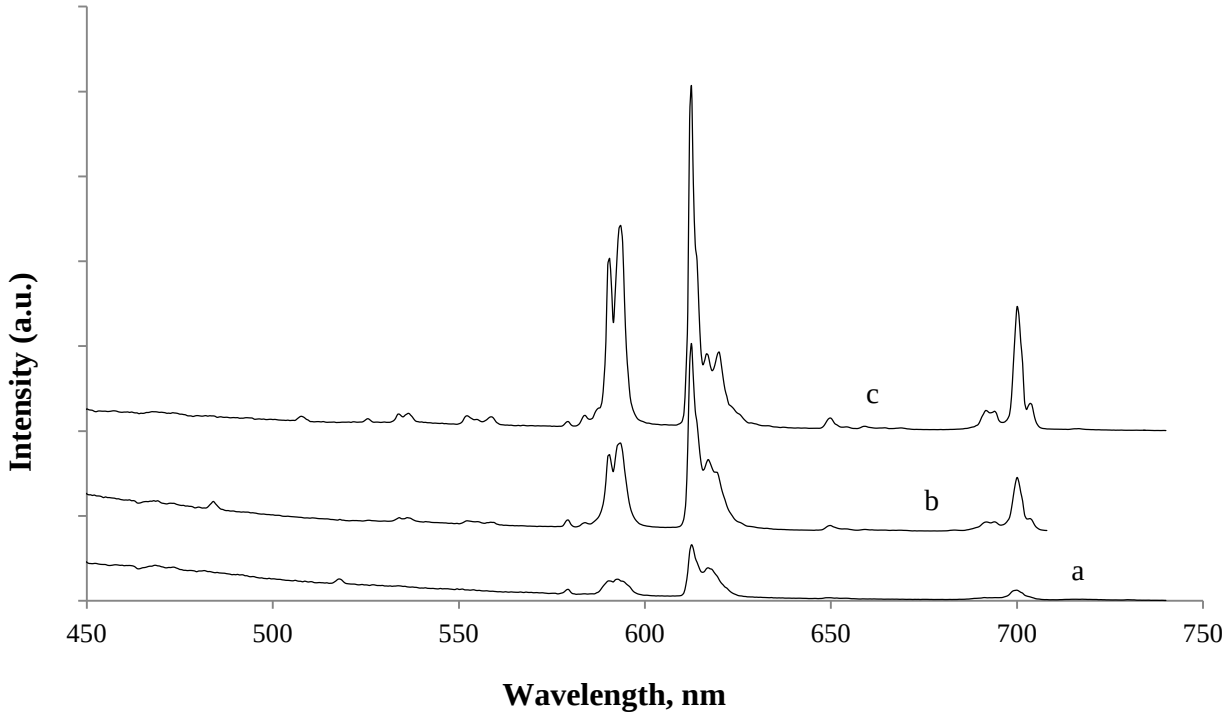


*Figure 3.8.* Emission spectra of $[Eu(TPAO)_2(H_2O)_6]Cl_3$ collected at liquid $N_2$ temperature upon excitation with: (a) 390, (b) 364, (c) 382 nm.

Table 3.3

*Assignment of Bands for $Eu^{3+}$ Excitation Spectra of the $[Eu(TPAO)_2(H_2O)_6]Cl_3$ complex.*

| **Energy ($cm^{-1}$)** | **Wavelength (nm)** | **Assignment** |
|---|---|---|
| 28570 | 350 | $^5L_9 \leftarrow {}^7F_0$ |
| 27700 | 361 | $^5G_2 \leftarrow {}^7F_0$ |
| 27470 | 364 | $^5G_2 \leftarrow {}^7F_0$ |
| 26180 | 382 | $^5L_6 \leftarrow {}^7F_0$ |
| 26040 | 384 | $^5L_6 \leftarrow {}^7F_0$ |
| 22080 | 453 | $^5D_2 \leftarrow {}^7F_0$ |
| 21650 | 462 | $^5D_2 \leftarrow {}^7F_0$ |
| 19460 | 514 | $^5D_1 \leftarrow {}^7F_0$ |

Table 3.4

*Assignment of Bands for $Eu^{3+}$ Emission Spectra of the $[Eu(TPAO)_2(H_2O)_6]Cl_3$ complex.*

| **Energy ($cm^{-1}$)** | **Wavelength (nm)** | **Assignment** |
|---|---|---|
| 19720 | 507 | $^5D_1 \rightarrow {}^7F_0$ |
| 19050 | 525 | $^5D_1 \rightarrow {}^7F_0$ |
| 18760 | 533 | $^5D_1 \rightarrow {}^7F_1$ |
| 18660 | 535 | $^5D_1 \rightarrow {}^7F_1$ |
| 18120 | 552 | $^5D_1 \rightarrow {}^7F_1$ |
| 17920 | 558 | $^5D_1 \rightarrow {}^7F_1$ |
| 17270 | 578 | $^5D_0 \rightarrow {}^7F_0$ |

Table 3.4 *(cont).*

| **Energy ($cm^{-1}$)** | **Wavelength (nm)** | **Assignment** |
|---|---|---|
| 17150 | 583 | $^5D_0 \rightarrow {}^7F_0$ |
| 17050 | 587 | $^5D_0 \rightarrow {}^7F_1$ |
| 16950 | 589 | $^5D_0 \rightarrow {}^7F_1$ |
| 16890 | 593 | $^5D_0 \rightarrow {}^7F_1$ |
| 16340 | 612 | $^5D_0 \rightarrow {}^7F_2$ |
| 16210 | 616 | $^5D_0 \rightarrow {}^7F_2$ |
| 16160 | 619 | $^5D_0 \rightarrow {}^7F_2$ |
| 15380 | 649 | $^5D_0 \rightarrow {}^7F_3$ |
| 14470 | 691 | $^5D_0 \rightarrow {}^7F_4$ |
| 14430 | 693 | $^5D_0 \rightarrow {}^7F_4$ |
| 14310 | 699 | $^5D_0 \rightarrow {}^7F_1$ |
| 14220 | 703 | $^5D_0 \rightarrow {}^7F_4$ |

### 3.6 Infrared Spectroscopy of $[Eu(TPAO)_4(H_2O)_4]Cl_3$

The IR spectral data shown below in Figure 3.9 was collected up to 5000 $cm^{-1}$. The specific frequencies that are characteristic of $[Eu(TPAO)_4(H_2O)_4]Cl_3$ complex are displayed. The IR spectra indicated the presence of a broad $\nu_{OH}$ stretch at 3360 $cm^{-1}$. The $\nu_{CN}$ stretch is present at 1150 $cm^{-1}$. The aliphatic $sp^3$ hybridized $\nu_{CH}$ stretching is not seen below 3000 $cm^{-1}$ as a result of overlapping of the broad $\nu_{OH}$ stretching.

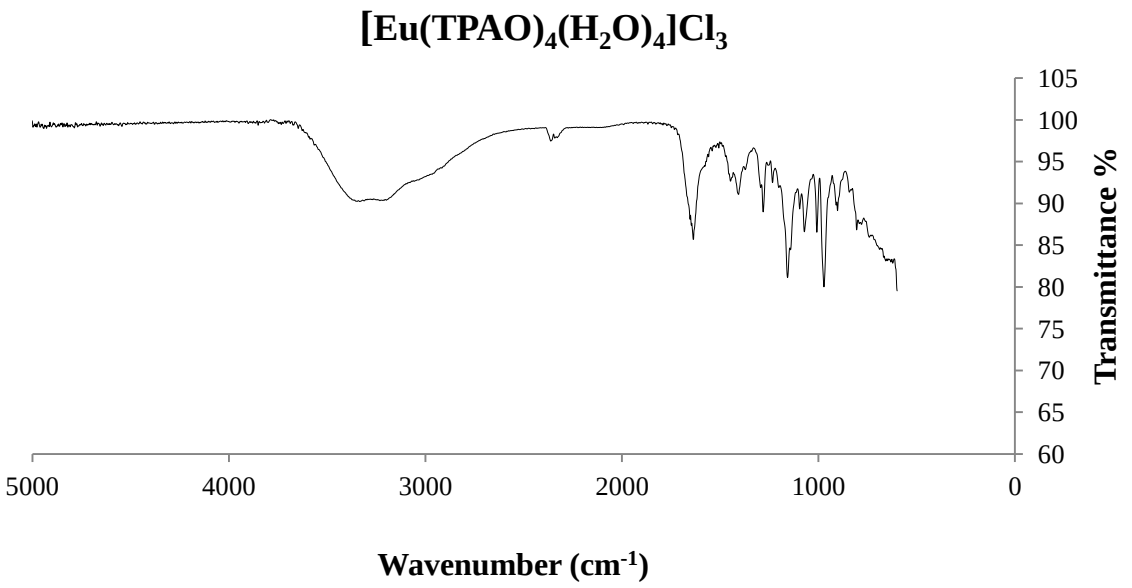


*Figure 3.9.* IR spectrum of $[Eu(TPAO)_4(H_2O)_4]Cl_3$

### 3.7 Photoluminescence Studies of $[Eu(TPAO)_4(H_2O)_4]Cl_3$

The excitation spectra of $[Eu(TPAO)_4(H_2O)_4]Cl_3$ shown in Figure 3.10 has a range from 320 nm to 520 nm. The spectra were collected at liquid $N_2$ temperature while monitoring at 592, 612, 616, and 699 nm. A sharp peak is observed at 382 nm when the excitation was monitored at 612 nm emission band. The excitation spectra of **[**$Eu(TPAO)_4(H_2O)_4]Cl_3$ presents two peaks in the $^5D_2$ -$^7F_0$ transition. An intense peak in the $^5L_6$ -$^7F_0$ region is observed at 382 nm. Tables 3.5 and 3.6 display the energies of $[Eu(TPAO)_4(H_2O)_4]Cl_3$ along with their assignments.

Figure 3.11 is the emission spectra of $[Eu(TPAO)_4(H_2O)_4]Cl_3$ with excitation at 453, 390, 364, and 382 nm for figures a, b, c, and d respectively. The spectra were collected at liquid $N_2$ temperature. The emission spectra of $[Eu(TPAO)_4(H_2O)_4]Cl_3$ display sharp emission lines characteristic of $Eu^{3+}$ f-f transition. Two peaks are observed in the $^5D_0 - {}^7F_0$, $^7F_1$ transition. The peaks present from 612 -616 nm correspond to the $^5D_0 - {}^7F_2$ transition. The $^5D_0 - {}^7F_2$ transitions are more intense which indicates an electronic dipole transition. Peaks seen in the 650-699 nm range are attributed to the $^5D_0 - {}^7F_3$, $^7F_4$ transitions.

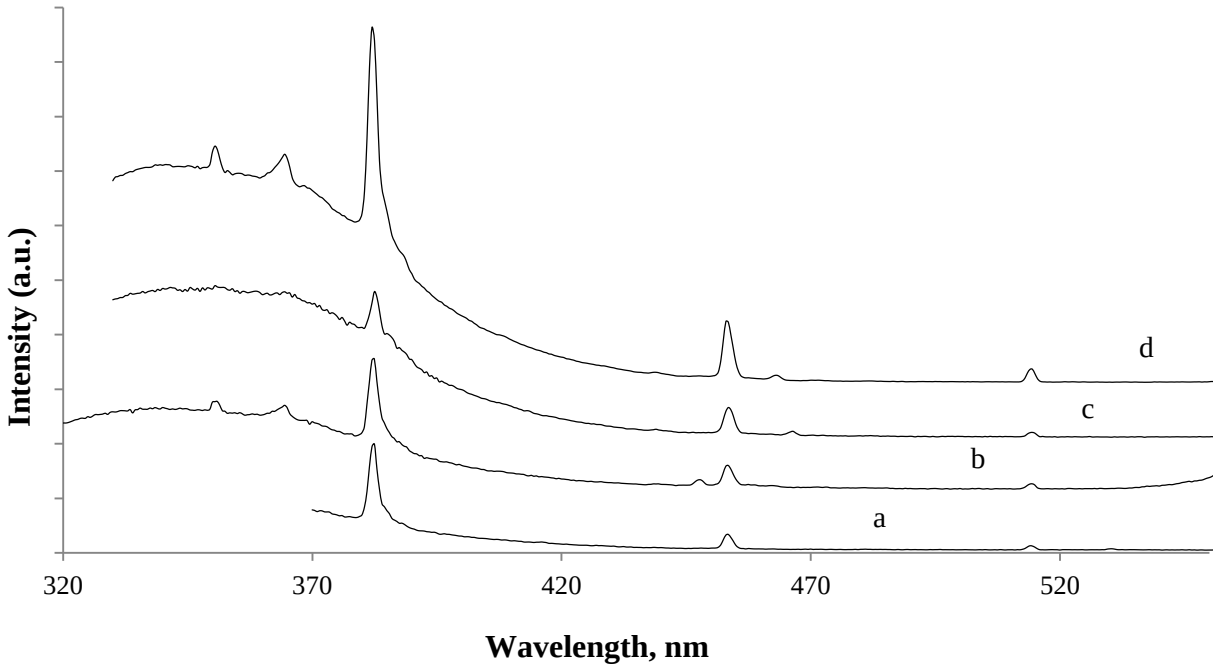


*Figure 3.10.* Excitation spectra of $[Eu(TPAO)_4(H_2O)_4]Cl_3$ collected at liquid $N_2$ temperature by monitoring the emission at: (a) 699, (b) 592, (c) 616, (d) 612 nm.

Table 3.5

Assignment of Bands for $Eu^{3+}$ Excitation Spectra of the $[Eu(TPAO)_4(H_2O)_4]Cl_3$ complex.

| **Energy ($cm^{-1}$)** | **Wavelength (nm)** | **Assignment** |
|---|---|---|
| 28570 | 349 | $^5L_6 \leftarrow {}^7F_0$ |
| 27470 | 364 | $^5L_6 \leftarrow {}^7F_0$ |
| 26180 | 382 | $^5L_6 \leftarrow {}^7F_0$ |
| 22120 | 453 | $^5D_2 \leftarrow {}^7F_0$ |
| 21600 | 462 | $^5D_2 \leftarrow {}^7F_0$ |
| 19460 | 513 | $^5D_1 \leftarrow {}^7F_0$ |

Table 3.6

*Assignment of Bands for $Eu^{3+}$ Emission Spectra of the $[Eu(TPAO)_4(H_2O)_4]Cl_3$ complex.*

| **Energy ($cm^{-1}$)** | **Wavelength (nm)** | **Assignment** |
|---|---|---|
| 17300 | 579 | $^5D_0 \rightarrow {}^7F_0$ |
| 17150 | 583 | $^5D_0 \rightarrow {}^7F_0$ |
| 17010 | 588 | $^5D_0 \rightarrow {}^7F_1$ |
| 16860 | 593 | $^5D_0 \rightarrow {}^7F_1$ |
| 16340 | 612 | $^5D_0 \rightarrow {}^7F_2$ |
| 16210 | 616 | $^5D_0 \rightarrow {}^7F_2$ |
| 15410 | 650 | $^5D_0 \rightarrow {}^7F_3$ |
| 15310 | 653 | $^5D_0 \rightarrow {}^7F_3$ |
| 14510 | 689 | $^5D_0 \rightarrow {}^7F_4$ |
| 14410 | 694 | $^5D_0 \rightarrow {}^7F_4$ |
| 14310 | 699 | $^5D_0 \rightarrow {}^7F_4$ |

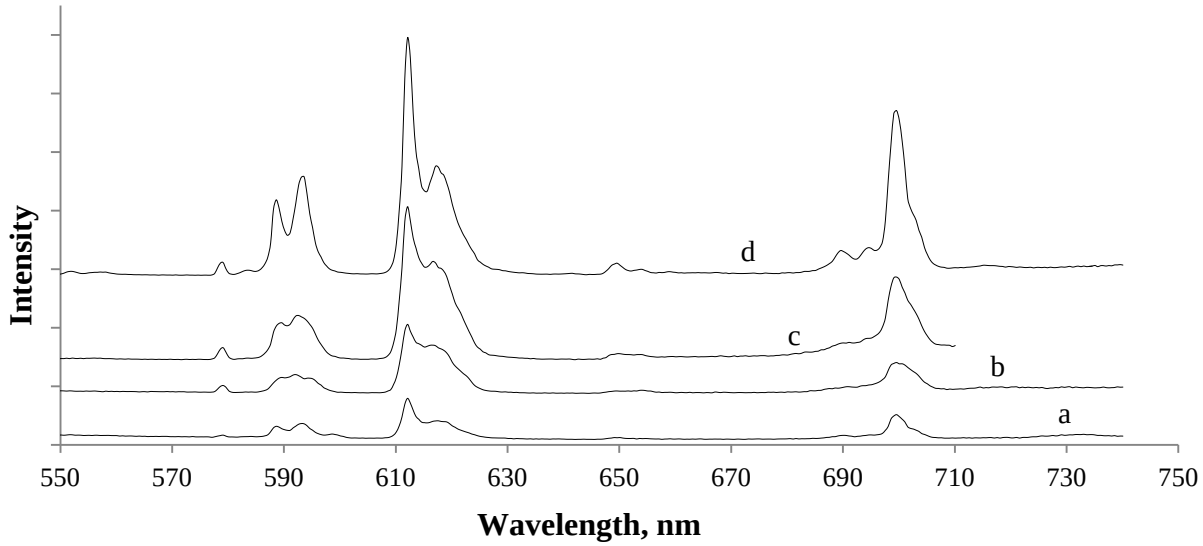


*Figure 3.11.* Emission spectra of $[Eu(TPAO)_4(H_2O)_4]Cl_3$ collected at liquid $N_2$ temperature.

Excited with: (a) 453, (b) 390, (c) 364, (d) 382 nm.

### 3.8 Infrared Spectroscopy of $[Tb(TPAO)_2(H_2O)_6]Cl_3$

The IR data shown below in Figure 3.12 displays specific frequencies that are characteristic of $[Tb(TPAO)_2(H_2O)_6]Cl_3$ complex. The IR spectra indicated the presence of $\nu_{OH}$ at 3270 $cm^{-1}$. The $\nu_{CN}$ stretch is visible at 1170 and 1160 $cm^{-1}$. The $sp^3$ hybridized $\nu_{CH}$ stretching is observed at 2870 $cm^{-1}$, albeit very weak band.

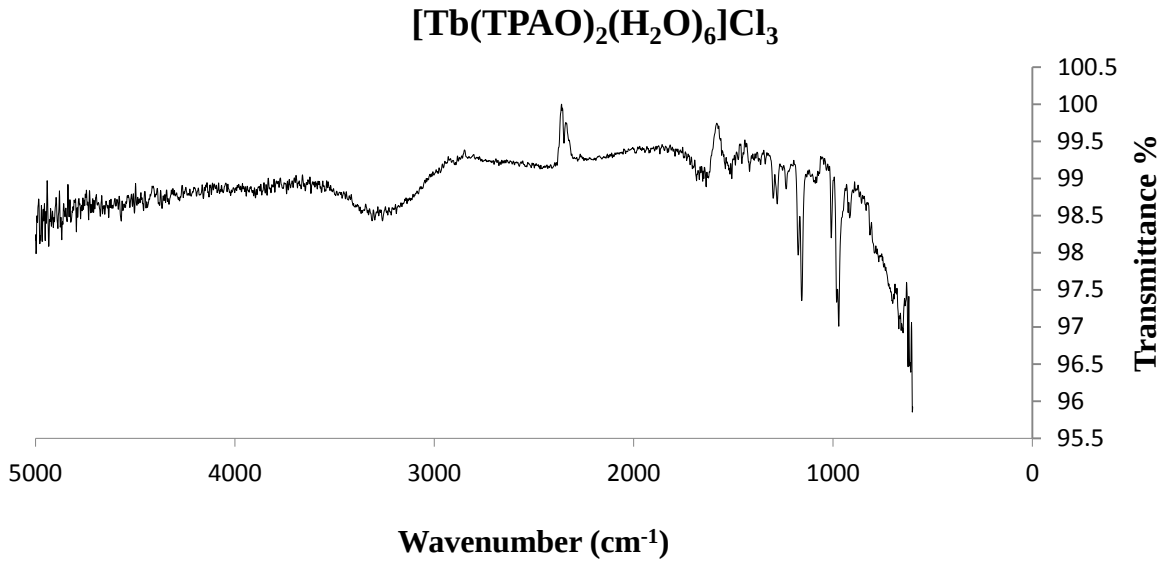


*Figure 3.12.* IR spectrum of $[Tb(TPAO)_2(H_2O)_6]Cl_3$

### 3.9 Photoluminescence Studies of $[Tb(TPAO)_2(H_2O)_6]Cl_3$

The excitation spectra of $[Tb(TPAO)_2(H_2O)_6]Cl_3$ shown in Figure 3.13 in the spectral range of 270 nm to 530 nm. Sharp bands at 348, 356, 367, and 374 nm overlay a broad band at 335 nm. The excitation spectra were monitored both at 489 nm and 542 nm emission band in figure 3.13. The excitation and emission spectra were both collected at liquid $N_2$ temperature. Figure 3.14 corresponds to the emission spectra of $[Tb(TPAO)_2(H_2O)_6]Cl_3$ with the excitation monitored at 333, 350, 367, and 375 nm for figures a, b, c, and d, respectively. Sharp peaks are observed at 488, 540, 542,545, 548, 581, 588, and 621nm which are characteristics of $Tb^{3+}$ f-f transitions corresponding to $^5D_4 \rightarrow {}^7F_0$.

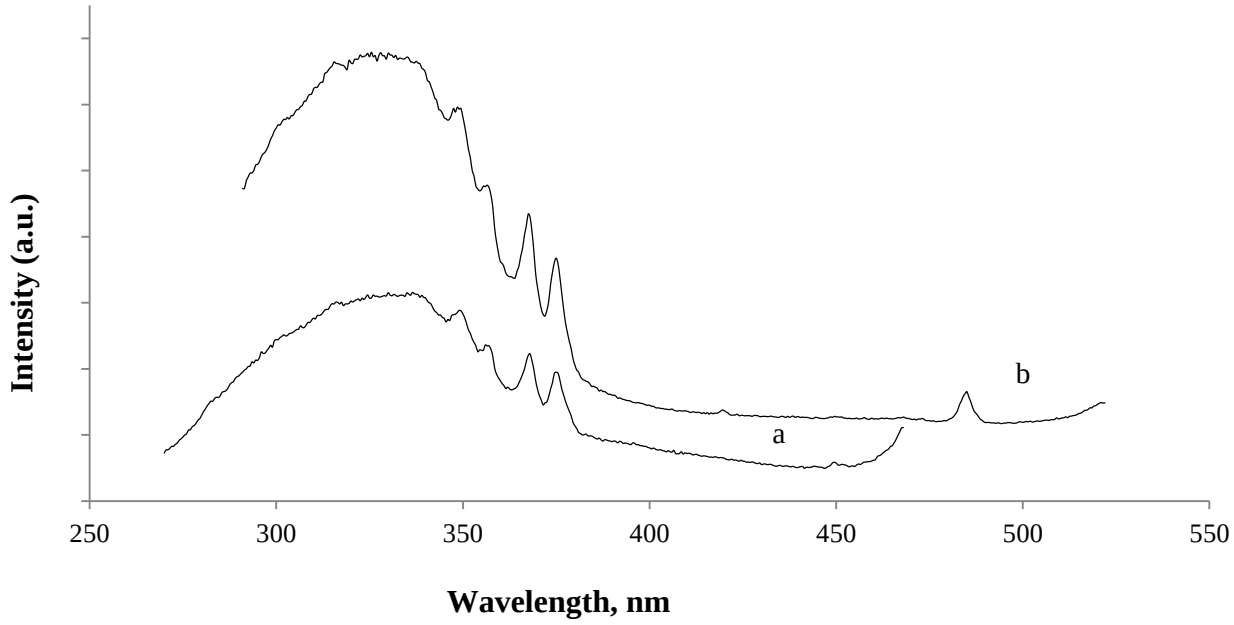


*Figure 3.13.* Excitation spectra of $[Tb(TPAO)_2(H_2O)_6]Cl_3$ collected at liquid $N_2$ temperature by monitoring the emission at: (a) 489, (b) 542 nm.

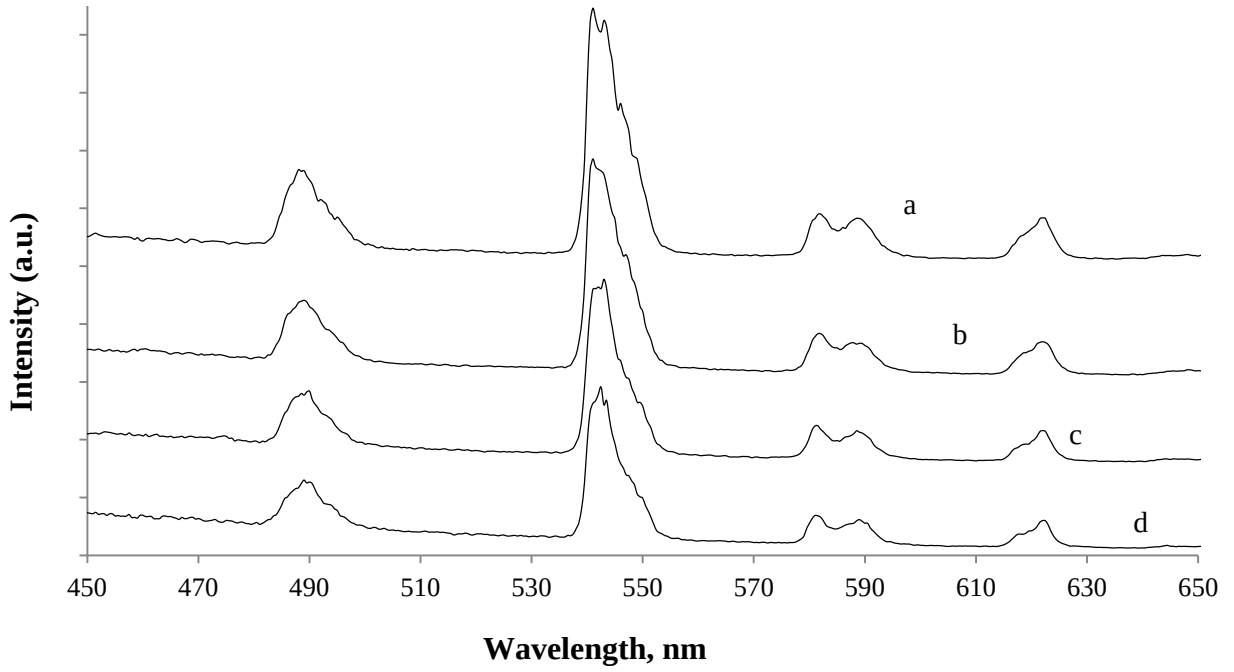


*Figure 3.14.* Emission spectra of $[Tb(TPAO)_2(H_2O)_6]Cl_3$ collected at liquid $N_2$ temperature by monitoring the excitation at: (a) 333, (b) 350, (c) 367, (d) 374 nm.

A broad band is displayed at 335 nm in the excitation spectrum of $[Tb(TPAO)_2(H_2O)_6]Cl_3$ complex which corresponds to the $^5D_2 \leftarrow {}^7F_6$ transition. Two other peaks at 348 and 356 nm also are assigned to this $^5D_3 \leftarrow {}^7F_6$ region transition. Two sharp peaks are also observed in the Table 3.7 which shows the excitation energies along with the assignments for the peaks.

Upon photoexcitation $Tb^{3+}$ ion is known by its most prominent green emission corresponding to the $^5D_4 \rightarrow {}^7F_5$ transition. The green emission band splits into two peaks at 540 and 542 nm which is consistent with the $^5D_4 \rightarrow {}^7F_5$ transition assignment. In addition a peak is observed at 488 nm corresponding to the $^5D_4 \rightarrow {}^7F_6$ transition. In the $^5D_4 \rightarrow {}^7F_4$ region, two weak peaks are observed at 581 and 588 nm. The $^5D_4 \rightarrow {}^7F_6$ electronic transition band at 540 nm is a 4f-4f transition that is parity forbidden. Table 3.8 displays the emission energies of $[Tb(TPAO)_2(H_2O)_6]Cl_3$ along with their assignments.

Table 3.7

*Assignment of Bands for $Tb^{3+}$ Excitation Spectra of the $[Tb(TPAO)_2(H_2O)_6]Cl_3$ complex.*

| **Energy ($cm^{-1}$)** | **Wavelength (nm)** | **Assignment** |
|---|---|---|
| 29850 | 335 | $^5D_2 \leftarrow {}^7F_6$ |
| 28740 | 348 | $^5D_2 \leftarrow {}^7F_6$ |
| 28090 | 356 | $^5D_2 \leftarrow {}^7F_6$ |
| 27250 | 367 | $^5D_3 \leftarrow {}^7F_6$ |
| 26740 | 374 | $^5D_3 \leftarrow {}^7F_6$ |
| 20620 | 485 | $^5D_4 \leftarrow {}^7F_6$ |

Table 3.8

*Assignment of Emission Bands for $Tb^{3+}$ ion in $[Tb(TPAO)_2(H_2O)_6]Cl_3$ complex.*

| **Energy ($cm^{-1}$)** | **Wavelength (nm)** | **Assignment** |
|---|---|---|
| 20490 | 488 | $^5D_4 \rightarrow {}^7F_6$ |
| 18520 | 540 | $^5D_4 \rightarrow {}^7F_5$ |
| 18450 | 542 | $^5D_4 \rightarrow {}^7F_5$ |
| 18350 | 545 | $^5D_4 \rightarrow {}^7F_5$ |
| 18250 | 548 | $^5D_4 \rightarrow {}^7F_5$ |
| 17210 | 581 | $^5D_4 \rightarrow {}^7F_4$ |
| 17000 | 588 | $^5D_4 \rightarrow {}^7F_4$ |
| 16100 | 621 | $^5D_4 \rightarrow {}^7F_3$ |

### 3.10 Infrared Spectroscopy of $[Tb(TPAO)_4(H_2O)_4]Cl_3$

The IR data ranging up to 5000 $cm^{-1}$ is shown below in Figure 3.15. The specific frequencies that are characteristic of $[Tb(TPAO)_4(H_2O)_4]Cl_3$ complex are displayed. In the IR spectra the presence of a broad $\nu_{OH}$ stretch at 3240 $cm^{-1}$ is indicated. The $\nu_{CN}$ stretch is observed at 1150 $cm^{-1}$. The aliphatic $sp^3$ hybridized $\nu_{CH}$ stretching is weakly observed presumably due to overlapping with the broad $\nu_{OH}$ stretching.

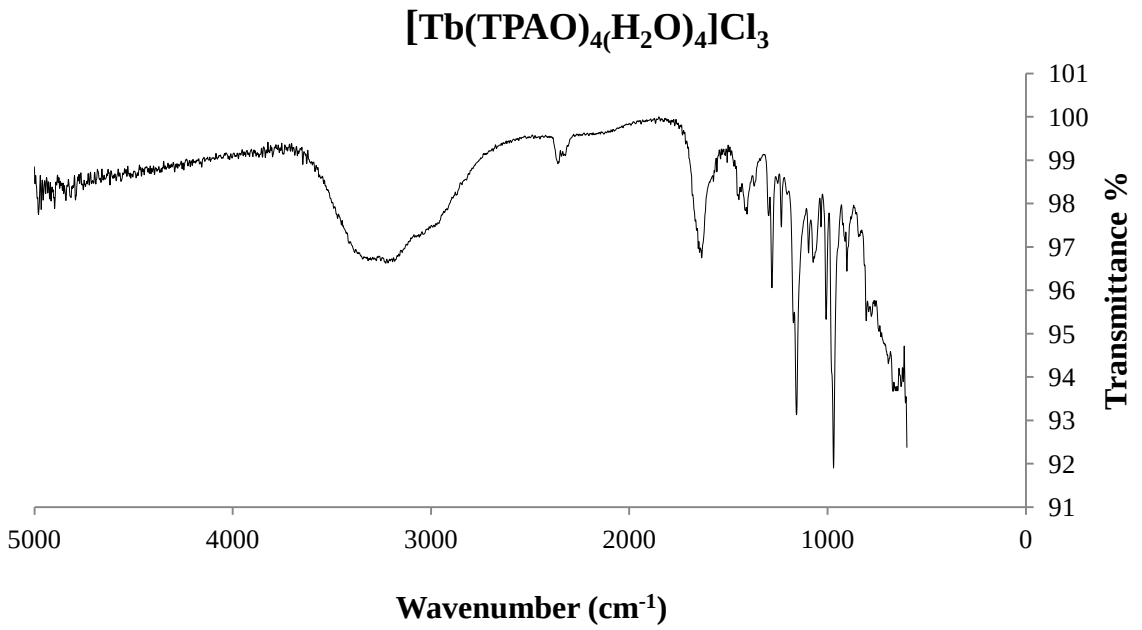


*Figure 3.15.* IR spectrum of $[Tb(TPAO)_4(H_2O)_4]Cl_3$

### 3.11 Photoluminescence Studies of $[Tb(TPAO)_4(H_2O)_4]Cl_3$

Figure 3.16 shows the excitation spectra of $[Tb(TPAO)_4(H_2O)_4]Cl_3$ collected at liquid $N_2$ temperature. The emission was monitored at 488 nm and 542 nm, covering the spectral region from 270 to 500 nm. The emission spectra of $[Tb(TPAO)_4(H_2O)_4]Cl_3$ is shown in Figure 3.17. The excitation was observed at 350, 356, 367, and 374 nm.

The excitation spectra the $[Tb(TPAO)_4(H_2O)_4]Cl_3$ complex displays a broad peak at 330 nm which is located in the $^5D_2 \leftarrow {}^7F_6$ transition region. Two shoulder peaks are also evident in this region at 348 and 355 nm. The $^5D_3 \leftarrow {}^7F_6$ transition region shows two sharp peaks at 367 and 374 nm. Table 3.9 presents the excitation energy bands and their assignments. In the emission spectra of $[Tb(TPAO)_4(H_2O)_4]Cl_3$ seven peaks are observed with the most intense peak located at 543 nm. A shoulder peak is at 540 nm is visible. In the $^5D_4 \rightarrow {}^7F_5$ transition region two peaks are displayed. Table 3.10 displays the assignment for the $Tb^{3+}$ emission spectra of $[Tb(TPAO)_4(H_2O)_4]Cl_3$ complex.

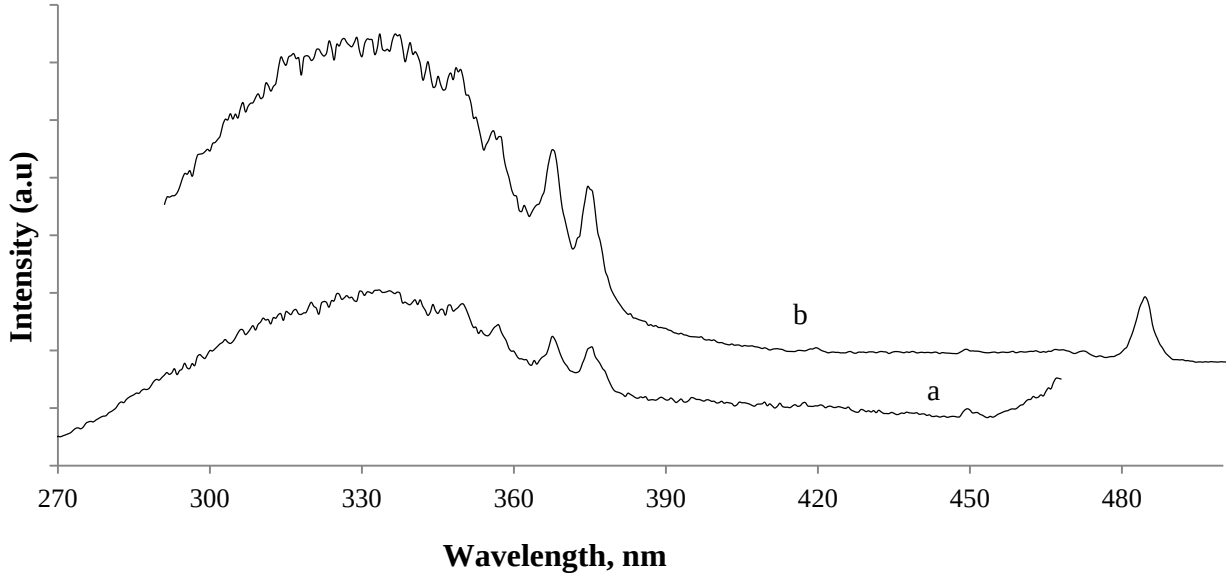


*Figure 3.16.* Excitation spectra of $[Tb(TPAO)_4(H_2O)_4]Cl_3$ collected at liquid $N_2$ temperature upon monitoring the emission at: (a) 488, (b) 542nm.

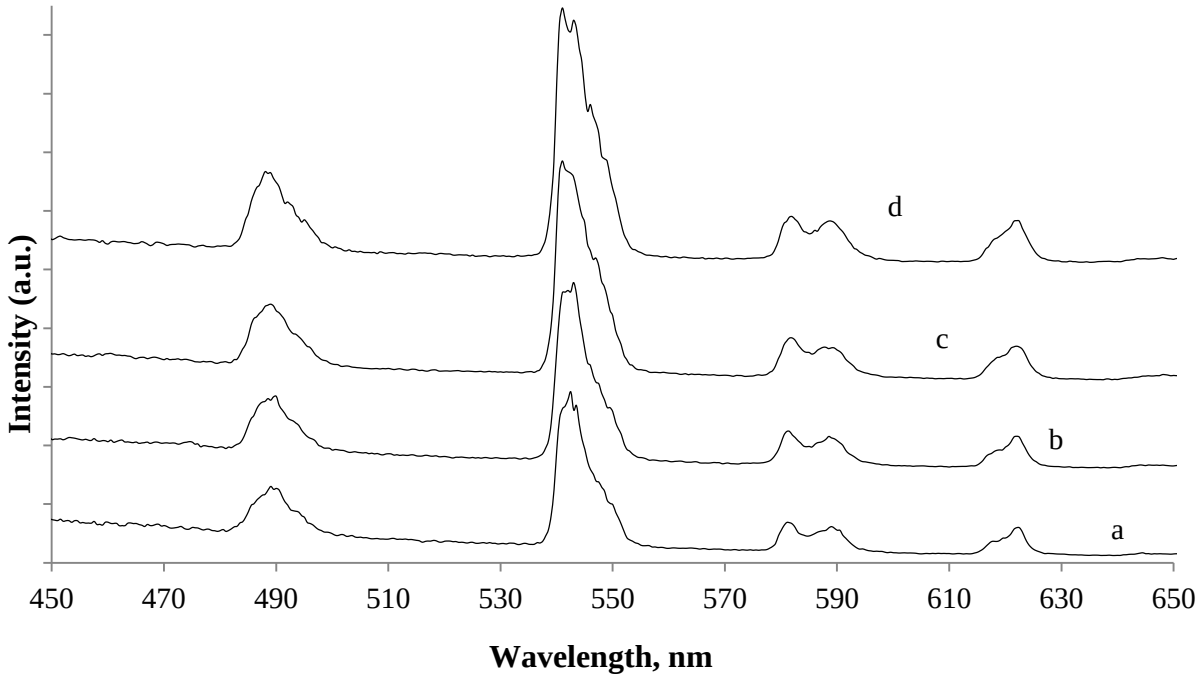


*Figure 3.17.* Emission spectra of $[Tb(TPAO)_4(H_2O)_4]Cl_3$ collected at liquid $N_2$ temperature upon monitoring the excitation at: (a) 374, (b) 367, (c) 356, (d) 350 nm.

Table 3.9
*Assignment of Bands for $Tb^{3+}$ Excitation Spectra of the $[Tb(TPAO)_4(H_2O)_4]Cl_3$ complex.*

| **Energy ($cm^{-1}$)** | **Wavelength (nm)** | **Assignment** |
|---|---|---|
| 30400 | 329 | $^5D_2 \leftarrow {}^7F_6$ |
| 28740 | 348 | $^5D_2 \leftarrow {}^7F_6$ |
| 28170 | 355 | $^5D_2 \leftarrow {}^7F_6$ |
| 27250 | 367 | $^5D_3 \leftarrow {}^7F_6$ |
| 26740 | 374 | $^5D_3 \leftarrow {}^7F_6$ |
| 20620 | 485 | $^5D_4 \leftarrow {}^7F_6$ |

Table 3.10

*Assignment of Bands for $Tb^{3+}$ Emission Spectra of the $[Tb(TPAO)_4(H_2O)_4]Cl_3$ complex.*

| **Energy ($cm^{-1}$)** | **Wavelength (nm)** | **Assignment** |
|---|---|---|
| 20490 | 488 | $^5D_4 \rightarrow {}^7F_6$ |
| 20320 | 492 | $^5D_4 \rightarrow {}^7F_6$ |
| 18520 | 540 | $^5D_4 \rightarrow {}^7F_5$ |
| 18420 | 543 | $^5D_4 \rightarrow {}^7F_5$ |
| 17180 | 582 | $^5D_4 \rightarrow {}^7F_4$ |
| 16970 | 589 | $^5D_4 \rightarrow {}^7F_4$ |
| 16080 | 622 | $^5D_4 \rightarrow {}^7F_3$ |

### 3.12 Infrared Spectroscopy of $Tb(Au(CN)_2)_3(Terpy)\cdot 4H_2O$

The IR data shown below in Figure 3.18 displays specific frequencies that are characteristic to the $Tb(Au(CN)_2)_3(Terpy)\cdot 4H_2O$ complex. The IR spectra indicated the presence of $\nu_{CN}$ stretching at 2130, 2150, 2170 $cm^{-1}$. The presence of an aromatic $-NR_2$ is also indicated.

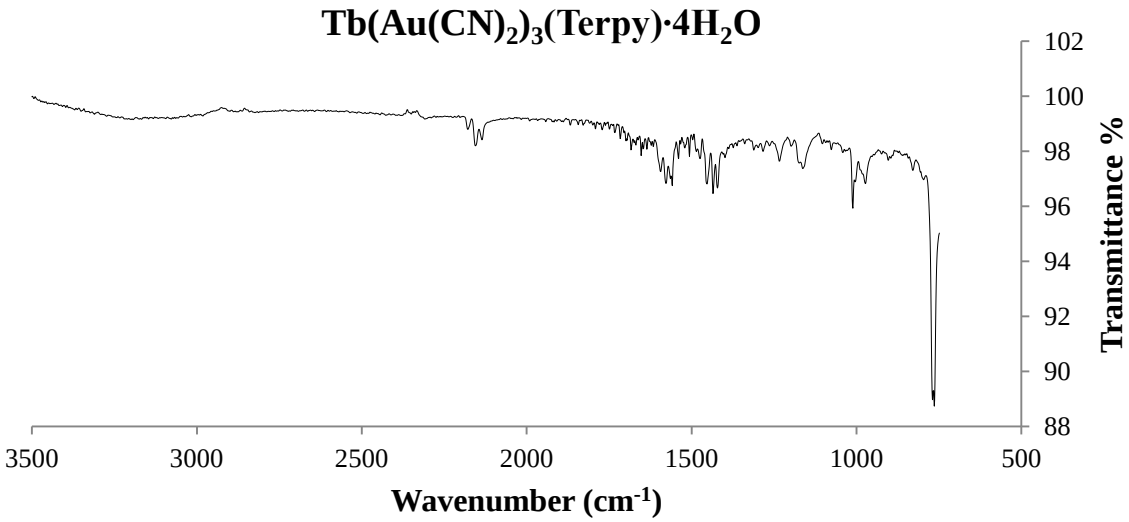


*Figure 3.18.* IR spectrum of $Tb(Au(CN)_2)_3(Terpy)\cdot 4H_2O$

### 3.13 Crystal Structure of $Tb(Au(CN)_2)_3(Terpy)\cdot 4H_2O$

Another area of this research effort involves the rational choice of multiple donors that can be excited concurrently for *cooperative sensitization application.* Two classes of donor groups have been studied. On one hand N-containing multidentate donor ligands including bipy, terpy, benzimidazole amides, phenanthroline amides, and other imidazole based cyclic amines were planned, but only the terpy ligand was studied in detail. The second class of donors planned involved selected group 10 and 11 transition metal complexes that will form direct coordination to the lanthanide center. To establish efficient cooperative mode, donor groups are chosen to display some common feature and maintain strongly overlapping absorption regions. In addition donors with large extinction coefficients, which can be fine-tuned through substituent effects, are chosen. The terpy ligand acts as light-harvesting antennae and can subsequently transfer

absorbed energy to coordinated $Ln^{3+}$ cations. Synthesis of complexes with two potential donors was achieved by combining the terpy ligand with that of group 11 metal complex, $Au(CN)_2^-$. A representative structure in this work is shown in Figure 3.19 on the Tb complex where successful synthesis and crystallization and structural refinement was achieved on the $Tb(Au(CN)_2)_3(Terpy)\cdot 4H_2O$ system. The unit cell parameters of Tb are a= 10.6419(17) b = 16.407(3) and c = 24.992(4) Å with $\alpha = 90^\circ$ $\beta = 98.535(5)^\circ$ and $\gamma = 90^\circ$. The compound crystallizes in the monoclinic crystal system and the space group is P 1 21/n1and Z = 4. At the time of preparation of this thesis the R1 value of this structure is 7.26%. A summary of the crystallographic data are given in Table 3.11, with a detailed list of the bond distances and angles given in Table 3.12. The Tb atom in the structure is coordinated to one terpy ligand, two dicyanoaurates, and four water molecules. The overall coordination environment of the Tb site is nine and geometry can be described as distorted antiprismatic. The structure also consists of a free uncoordinated terpy ligand in addition to three water molecules in the lattice. Four symmetry related molecules exist in the unit cell with along with four uncoordinated terpy ligands.

The four water molecules coordinated to the $Tb^{3+}$ ion have an average Tb-O bond distance of 2.442 Å. The Tb-N bond distances of the terpy are 2.53, 2.57, and 2.58 Å. While the Tb-N bond distances of cyanide ligand are 2.50 and 2.53 Å. The bond distance of Tb-N of the terpy and cyanide are on average similar. The terpy ligand acts as light-harvesting antennae and can subsequently transfer absorbed energy to coordinated $Ln^{3+}$ cations.

The overall structural feature is fascinating in that the structure consist of two $[Au(CN)_2]^-$ anions coordinated directly to a $Tb^{3+}$ site through the N- atom of the cyanide ligand. A third $Au(CN)_2^-$ is also present in the lattice, albeit uncoordinated to the $Tb^{3+}$ center. This “free”

$Au(CN)_2^-$ ion is locked into the structure by aurophilic Au−Au interaction with M-M distances of 3.23 and 3.22 Å . The fascinating aspect of this structure is that the M-M-M angle is only 124.9°. The uncoordinated Au is placed ~ 1.5 Å above the plane of the two coordinated Au atoms. Neighboring molecules are inverted in orientation and an extended zig-zag chain is present in the structure which can be seen in Figure 3.20 of packing diagram with intermolecular Au-Au distance of 3.43 Å. Hence the molecule consists of a three metal cluster with extended zig –zag chain along a defined axis. The luminescence property of this compound has been studied and shows enhanced emission from the $Tb^{3+}$ ion although emission from the gold center is totally quenched both in room and liquid nitrogen temperature.

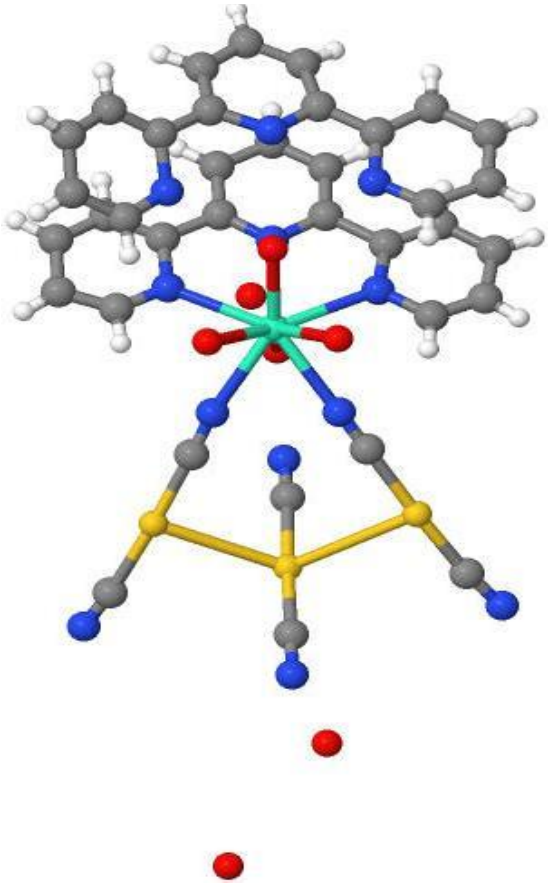

*Figure 3.19.* Crystal structure of $Tb(Au(CN)_2)_3(Terpy)\cdot 4H_2O$ illustrating the coordination environment of the $Tb^{3+}$ site.

Table 3.11

*Summary of the crystallographic data for $Tb(Au(CN)_2)_3(Terpy)\cdot 4H_2O$*

| | |
|---|---|
| Formula | $C_{36}H_{36}Au_3N_{12}O_7Tb$ |
| Mol. Wt. | 1498.59 |
| Dimensions ($mm^3$) | 0.200 x 0.550 x 0.600 |
| Crystal system | Monoclinic |
| Space Group | P 1 21/n 1 |
| a (Å) | 10.6419(17) |
| b (Å) | 16.407(3) |
| c (Å) | 24.992(4) |
| α (deg) | 90° |
| β (deg) | 98.535(5)° |
| γ (deg) | 90° |
| Volume $Å^3$ | 4315.3(12) |
| Temperature | 200(2)K |
| Z | 4 |
| Density (calculated) | 2.307 $Mg/cm^3$ |
| Absorption coefficient | 11.846 $mm^{-1}$ |
| Absorption correction | Multi-scan |
| F(000) | 2776 |
| Reflections collected | 40512 |
| Independent reflections | 3455 [R(int) = 0.3184] |
| Goodness-of-fit on $F^2$ | 0.963 |
| Final R indices [I>2σ(I)] | R1 = 0.0726, wR2 = 0.1744 |
| R indices (all data) | R1 = 0.0981, wR2 = 0.1895 |

$R_{int} = \Sigma| F_o^2 - F_o^2 (mean) | / \Sigma[F_o^2]$
$R_1 = \Sigma||F_o|- |F_c|| / \Sigma|F_o|$
$GOOF = S = \{\Sigma[w(F_o^2 - F_c^2)^2] / (n - p)\}^{1/2}$
$wR_2 = \{\Sigma[w(F_o^2 - F_c^2)^2] / \Sigma[w(F_o^2)^2]\}^{1/2}$
$w = 1 / [\sigma(F_o^2) + (aP)^2 + bP]$ where $P$ is $[2F_c^2 + Max(F_o^2, 0)] / 3$

Table 3.12

*Selected Bond Length (Å) and Angles (°) for $Tb(Au(CN)_2)_3(Terpy)\cdot 4H_2O$*

| | | | |
|---|---|---|---|
| Au1-Au2 | 3.23 | Au1-Au2-Au3 | 124.9 |
| Au2-Au3 | 3.22 | | |
| | | *N-C-Au | 172.4 |
| Tb1-O1 | 2.44 | | 174.8 |
| Tb1-O2 | 2.47 | | 178.1 |
| Tb1-O3 | 2.47 | | |
| Tb1-O4 | 2.39 | C-Au-C | 175.4 |
| | | | 176.6 |
| Tb1-N1 | 2.50 | | 177.4 |
| Tb1-N2 | 2.53 | | |
| Tb1-N3 | 2.53 | Au-C-N | 174.0 |
| Tb1-N4 | 2.57 | | 174.2 |
| Tb1-N5 | 2.58 | | 175.4 |

* Indicates N-C-Au not bonded through terbium center.

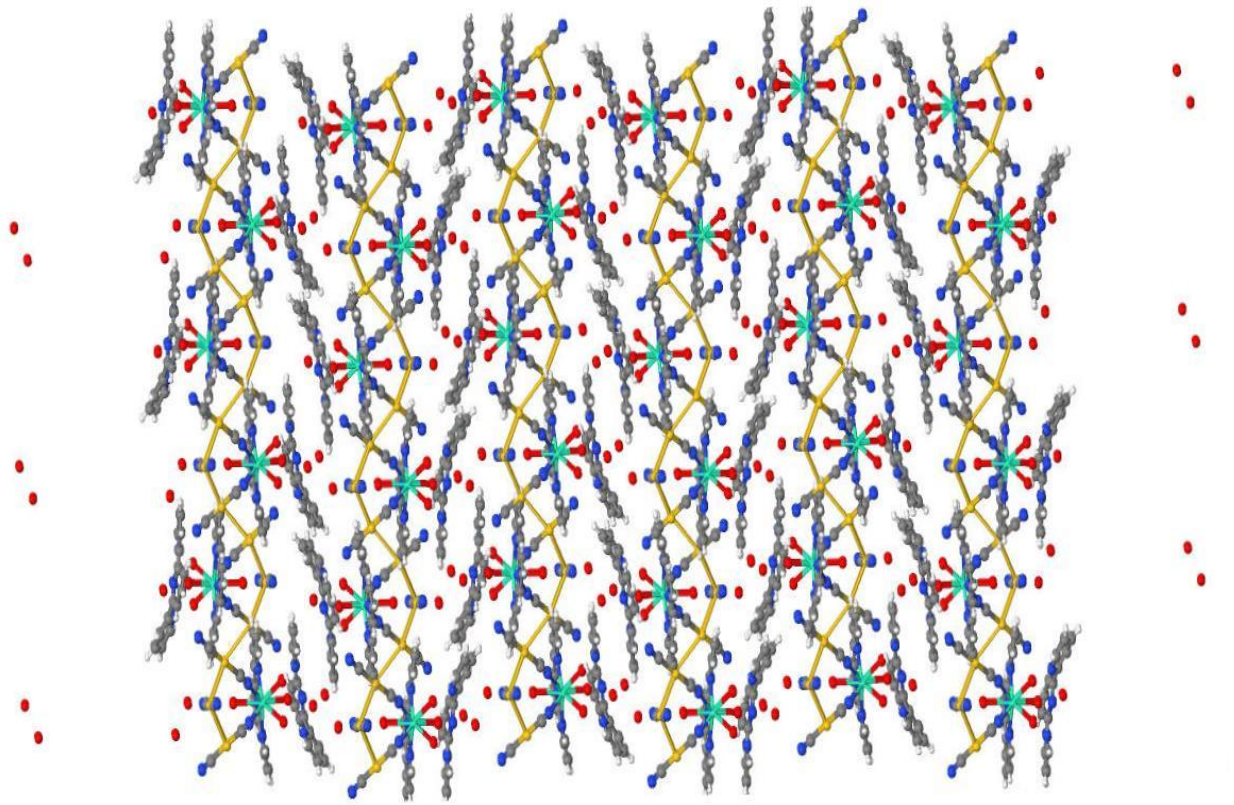

*Figure 3.20.* Extended zig-zag chain of Au atoms in $Tb(Au(CN)_2)_3(Terpy)\cdot 4H_2O$.

### 3.14 Photoluminescence Studies of $Tb(Au(CN)_2)_3(Terpy)\cdot 4H_2O$

The excitation spectra of $Tb(Au(CN)_2)_3(Terpy)\cdot 4H_2O$ shown in Figure 3.21 have a range from 270 nm to 550 nm. The spectra were collected at liquid $N_2$ temperature while monitoring at 620, 582, 542, and 489 nm. A broad band is observed at 350 nm in the excitation spectrum of $Tb(Au(CN)_2)_3(Terpy)\cdot 4H_2O$. The broad band is indicative to gold presence in the system. This band is assigned to $^5D_2 \leftarrow {}^7F_6$ transition. A small band is visible at 470 nm which corresponds to the blue region $^5D_4 \leftarrow {}^7F_6$transition. Table 3.13 displays the energies and assignment.

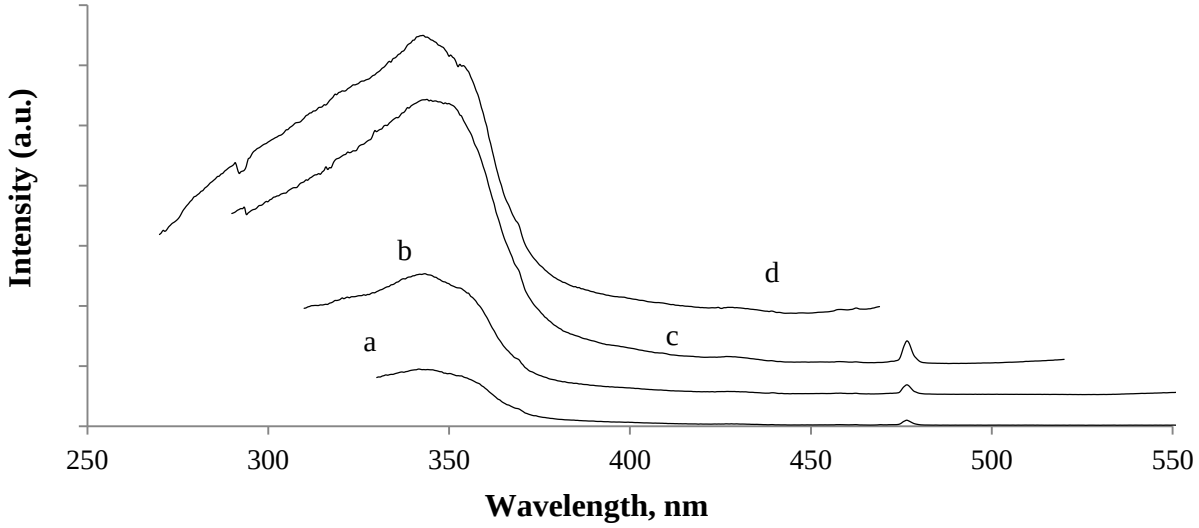


*Figure 3.21.* Excitation spectra of $Tb(Au(CN)_2)_3(Terpy)\cdot 4H_2O$ collected at liquid $N_2$ temperature by monitoring the emission at: (a) 620, (b) 582, (c) 542, (d) 489nm.

Table 3.13

*Assignment of Bands for $Tb^{3+}$ Excitation Spectra of the $Tb(Au(CN)_2)_3(Terpy)\cdot 4H_2O$ complex.*

| **Energy ($cm^{-1}$)** | **Wavelength (nm)** | **Assignment** |
|---|---|---|
| 29240 | 342 | $^5D_2 \leftarrow {}^7F_6$ |
| 21010 | 476 | $^5D_4 \leftarrow {}^7F_6$ |

Figure 3.22 is the emission spectra of $Tb(Au(CN)_2)_3(Terpy)\cdot 4H_2O$ with the excitation at 476, 360, and 342nm for figures a, b, and c respectively. Tables 3.14 displays the excitation and emission energies of $Tb(Au(CN)_2)_3(Terpy)\cdot 4H_2O$. The emission spectra of $Tb(Au(CN)_2)_3(Terpy)\cdot 4H_2O$ consist of sharp bands most intense at 542 nm and comparable to the $^5D_4 \rightarrow {}^7F_5$ transition. Three bands are observed in this transition region. In the $^5D_4 \rightarrow {}^7F_6$ region a peak can be seen at wavelength of 488 nm. The absence of a broad band in these emission spectra confirms that the energy from Au was transferred to terbium.

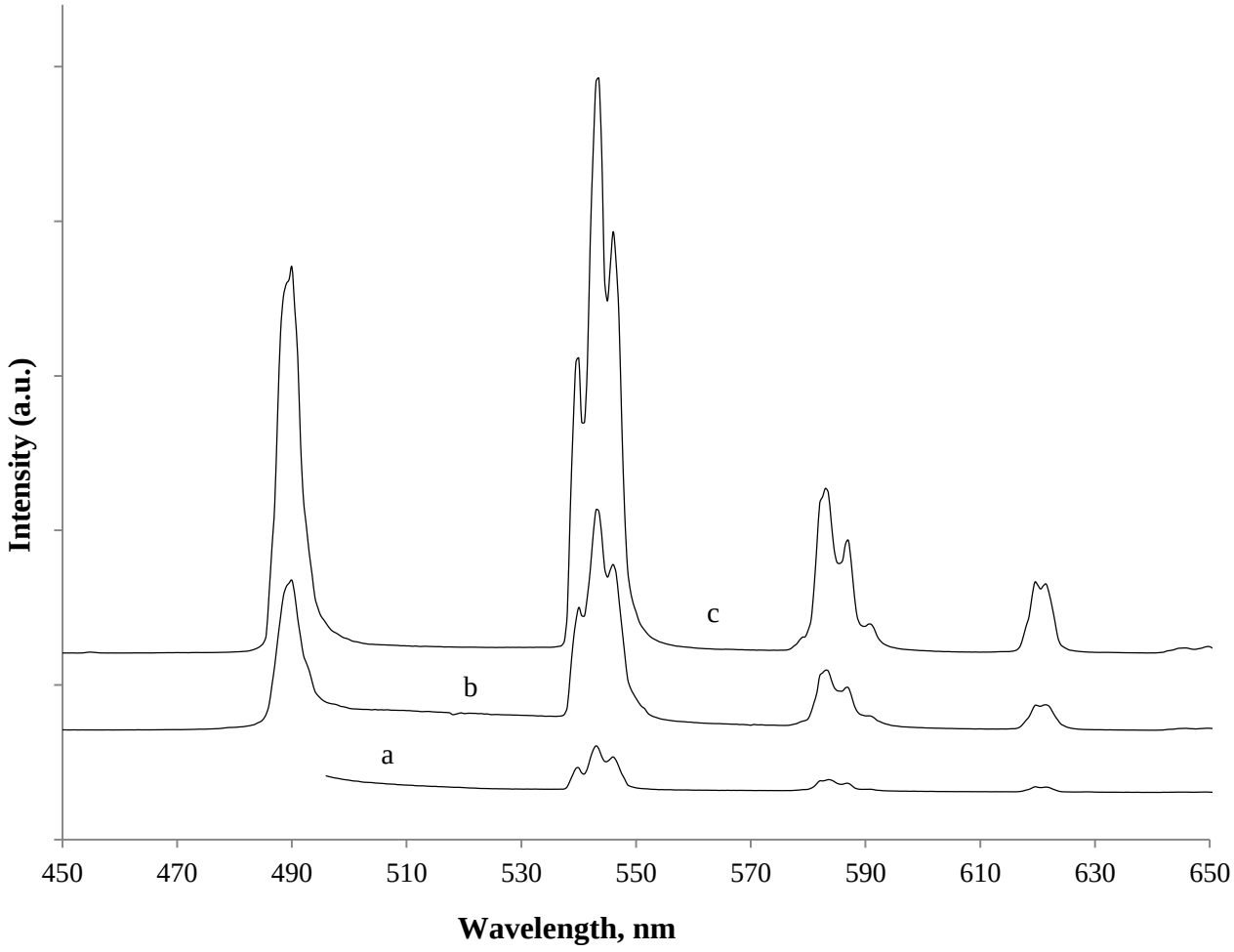


*Figure 3.22.* Emission spectra of $Tb(Au(CN)_2)_3(Terpy)\cdot 4H_2O$ collected at liquid $N_2$ temperature by monitoring the excitation at: (a) 476, (b) 360, (c) 342 nm.

Table 3.14

*Assignment of Bands for $Tb^{3+}$ Emission Spectra of the $Tb(Au(CN)_2)_3(Terpy)\cdot 4H_2O$ complex.*

| **Energy ($cm^{-1}$)** | **Wavelength (nm)** | **Assignment** |
|---|---|---|
| 20500 | 488 | $^5D_4 \rightarrow {}^7F_6$ |
| 18550 | 539 | $^5D_4 \rightarrow {}^7F_5$ |
| 18450 | 542 | $^5D_4 \rightarrow {}^7F_5$ |
| 18320 | 546 | $^5D_4 \rightarrow {}^7F_5$ |
| 17150 | 583 | $^5D_4 \rightarrow {}^7F_4$ |
| 17060 | 586 | $^5D_4 \rightarrow {}^7F_4$ |
| 16920 | 591 | $^5D_4 \rightarrow {}^7F_4$ |
| 16160 | 619 | $^5D_4 \rightarrow {}^7F_3$ |
| 16100 | 621 | $^5D_4 \rightarrow {}^7F_3$ |
| 15503 | 645 | $^5D_4 \rightarrow {}^7F_1$ |
| 15380 | 650 | $^5D_4 \rightarrow {}^7F_2$ |

# CHAPTER 4

## Conclusion

In conclusion, we have shown the successful coordination of up to two TPAO ligands to a $Eu^{3+}$ center via x-ray diffraction. The bis- TPAO was assigned a distorted square antiprism geometry with unit cell parameters of a = 35.992, b =10.0915, and c = 16.638 Å with $\alpha = \beta = \gamma = 90^{\circ}$. A shorter bond distance of the Eu-O with the TPAO ligand in comparison to the $H_2O$ ligand by 0.07Å deduces the stronger donor ability of the TPAO ligand. Modification of the phosphine oxide ligand is thought to take on a dual responsibility as effective sensitizers and replacement for the quencher $H_2O$. A crystal structure for the synthesis of these $Eu^{3+}$ and $Tb^{3+}$ complexes, $[Eu(TPAO)_4(H_2O)_4]Cl_3$, $[Tb(TPAO)_2(H_2O)_6]Cl_3$, $[Tb(TPAO)_4(H_2O)_4]Cl_3$ has not been obtained. Although, developing a synthetic scheme that may remove water completely from these lanthanide inner spheres is still in progress.

Development of multiple donor systems which can be excited simultaneously for cooperative sensitization is the other objective of this research project. In this regard in the $Tb(Au(CN)_2)_3(Terpy)\cdot 4H_2O$ complex the terpy and $Au(CN)_2^-$ anions are directly coordinated to the $Tb^{3+}$ ion and hence a dual-donor effect is exhibited. The successful synthesis, crystallization, and structural refinement were accomplished on this complex. The unit cell parameters of the complex is a =10.6419(17) b =16.407(3) and c =24.992(4) Å $\beta = 98.535(5)^{\circ}$ displaying a distorted antiprismatic geometry. $Tb(Au(CN)_2)_3(Terpy)\cdot 4H_2O$ complex shows an extended zig-zag chain of Au-Au interaction. The three $Au(CN)_2^-$ clustering around the Tb atom have a bond angle of only $124.9^{\circ}$ which made this a captivating compound.

References

[1] Harvey, E. N., A History of Luminescence. Philadelphia, American Philosophical Society: 1957.

[2] Bunzli, J.-C. G. "Taking advantage of luminescent lanthanide ions." *Chem. Soc. Rev.* **2005,** *34*, 1048-1077.

[3] Atkins, P., Physical Chemistry. 8th ed.; W.H Freeman and Company: New York, 2006.

[4] Elbanowski, M.; Makowska, B. "The lanthanides as luminescent probes in investigations of biochemical systems." *J. Photochem. Photobiol., A* **1996,** *99* (2-3), 85-92.

[5] Shriver, D. F. a. A., P.W., *Inorganic Chemistry*. 4th ed.; Oxford University Press: New York, 2006.

[6] Encyclopedia Britannica. In *Encyclopedia Britannica Online*, 2010.

[7] Dressler, L.; Dippe, M.; Ulbrich-Hofmann, R. "Lanthanides as activators and fluorescence probes of phospholipase D." *Chem. Phys. Lipids* **2010,** *163* (Supplement 1), S34-S34.

[8] Choppin, G. R.; Peterman, D. R. "Applications of lanthanide luminescence spectroscopy to solution studies of coordination chemistry." *Coord. Chem. Rev.* **1998,** *174* (1), 283-299.

[9] Cotton, S., Lanthanide and Actinide Chemistry. Wiley: 2006.

[10] Giraud, M.; Andreiadis, E. S.; Fisyuk, A. S.; Demadrille, R.; Pecaut, J.; Imbert, D.; Mazzanti, M. "Efficient Sensitization of Lanthanide Luminescence by Tetrazole-Based Polydentate Ligands." *Inorg. Chem.* **2008,** *47* (10), 3952-3954.

[11] Beatty, R., The Lanthanides. Marshall Cavendish Benchmark: New York, 2008.

[12] Rabie, K. A.; Sayed, S. A.; Lasheen, T. A.; Salama, I. E. "Europium separation from a middle rare earths concentrate derived from Egyptian black sand monazite." *Hydrometallurgy* **2007,** *86* (3-4), 121-130.

[13] Parker, D. "Luminescent lanthanide sensors for pH, pO2 and selected anions." *Coord. Chem. Rev.* **2000,** *205*, 109-130.

[14] T. Justel, H. N., C. Ronda "New development in the field of luminescent materials for lighting and displays." *Angew. Chem., Int. Ed.* **1998,** *37*, 3250.

[15] Richardson, F. S. "Terbium(III) and europium(III) ions as luminescent probes and stains for biomolecular systems." *Chem. Rev.* **1982,** *82* (5), 541-552.

[16] Changhao, Y. "Synthesis and Characterization of Rare Earth Complexes." *J. Rare Earths* **2007,** *25*, 117.

[17] Wegh, R. T.; Donker, H.; Oskam, K. D.; Meijerink, A. "Visible quantum cutting in Eu3+-doped gadolinium fluorides via downconversion." *J. Lumin.* **1999,** *82* (2), 93-104.

[18] Zamani, H. A.; Ganjali, M. R.; Norouzi, P.; Tadjarodi, A.; Shahsavani, E. "Determination of terbium(III) ions in phosphate rock samples by a $Tb^{3+}$-PVC membrane sensor based on N, N-Dimethyl-N', N''-bis(4-methoxyphenyl)phosphoramidate." *Mater. Sci. Eng.* **2008,** *28* (8), 1489-1494.

[19] Ortiz, C. P. Spectroscopy of Terbium doped Sol-gel Glasses. Davidson College, 2007.

[20] Forster, P. L.; Parra, D. F.; Kai, J.; Fermino, D. M.; Brito, H. F.; Lugao, A. B. "Effects of gamma radiation on the photoluminescence properties of polycarbonate matrices doped with terbium complex." *Radiat. Phys. Chem.* **2010,** *79* (3), 347-349.

[21] Liao, J.; Qiu, B.; Lai, H. "Synthesis and luminescence properties of $Tb^{3+}$:$NaGd(WO_4)_2$ novel green phosphors." *J. Lumin.* **2009,** *129* (7), 668-671.

[22] Martínez-Arias, A.; Hungría, A. B.; Fernández-García, M.; Iglesias-Juez, A.; Conesa, J. C.; Mather, G. C.; Munuera, G. "Cerium-terbium mixed oxides as potential materials for anodes in solid oxide fuel cells." *J. Power Sources* **2005,** *151*, 43-51.

[23] Geoffroy, G. L.; Denton, D. A.; Eigenbrot, C. W. "Photoinduced oxidation of tertiary arylphosphines." *Inorg. Chem.* **1976,** *15* (9), 2310-2311.

[24] Tolman, C. A. "Steric effects of phosphorus ligands in organometallic chemistry and homogeneous catalysis." *Chem. Rev.* **1977,** *77* (3), 313-348.

[25] Phillips, A. D.; Gonsalvi, L.; Romerosa, A.; Vizza, F.; Peruzzini, M. "Coordination chemistry of 1,3,5-triaza-7-phosphaadamantane (PTA): Transition metal complexes and related catalytic, medicinal and photoluminescent applications." *Coord. Chem. Rev.* **2004,** *248* (11-12), 955-993.

[26] Bolaño, S.; Albinati, A.; Bravo, J.; Gonsalvi, L.; Peruzzini, M. "Borane adducts of the water soluble phosphine PTA (PTA = 1,3,5-triaza-7-phosphaadamantane)." *Inorg. Chem. Commun.* **2006,** *9* (4), 360-363.

[27] Frost, B. J.; Lee, W.-C.; Pal, K.; Kim, T. H.; VanDerveer, D.; Rabinovich, D. "Synthesis, structure, and coordination chemistry of OPTA and SPTA with group 12 metals (PTA = 1,3,5-triaza-7-phosphaadamantane)." *Polyhedron* **2010,** *29* (11), 2373-2380.

[28] Wong, G. W.; Harkreader, J. L.; Mebi, C. A.; Frost, B. J. "Synthesis and Coordination Chemistry of a Novel Bidentate Phosphine: 6-(Diphenylphosphino)-1,3,5-triaza-7-phosphaadamantane (PTA-PPh2)." *Inorg. Chem.* **2006,** *45* (17), 6748-6755.

[29] Huang, R.; Frost, B. J. "Development of a Series of $P(CH_2NCHR)_3$ and Trisubstituted 1,3,5-Triaza-7-phosphaadamantane Ligands." *Inorg. Chem.* **2007,** *46* (26), 10962-10964.

[30] Hofmeier, H.; Schubert, U. S. "Recent developments in the supramolecular chemistry of terpyridine-metal complexes." *Chem. Soc. Rev.* **2004,** *33* (6), 373-399.

[31] Tong, B.-H.; Wang, S.-J.; Jiao, J.; Ling, F.-R.; Meng, Y.-Z.; Wang, B. "Novel luminescent lanthanide complexes covalently linked to a terpyridine-functionalized silica network." *J. Photochem. Photobiol., A* **2007,** *191* (1), 74-79.

[32] Hobert, S. E.; Carney, J. T.; Cummings, S. D. "Synthesis and luminescence properties of platinum(II) complexes of 4'-chloro-2,2':6',2"-terpyridine and 4,4',4"-trichloro-2,2':6',2"-terpyridine." *Inorg. Chim. Acta* **2001,** *318* (1-2), 89-96.

[33] Yam, V. W.-W.; Lo, K. K.-W. "Recent advances in utilization of transition metal complexes and lanthanides as diagnostic tools." *Coord. Chem. Rev.* **1999,** *184* (1), 157-240.

[34] Galaup, C.; Couchet, J. M.; Picard, C.; Tisnès, P. "Novel terpyridine macrocyclic complexing agent and luminescence of its neutral Ln(III) complexes (Ln=Eu, Tb, Sm, Dy) in aqueous solution." *Tetrahedron Lett.* **2001,** *42* (36), 6275-6278.

[35] Assefa, Z.; Patterson, H. H. "Photoluminescence studies of lanthanide ion complexes of gold and silver dicyanides. 2. A new low dimensional solid state class for nonradiative excited state energy transfer." *Inorg. Chem.* **1994,** *33* (26), 6194-6200.

[36] Guo, Z.; Yson, R. L.; Patterson, H. H. "Solvent dependent tunable energy transfer of d10 metal dicyanide nanoclusters with Eu3+ and Tb3+ rare earth ions." *Chem. Phys. Lett.* **2007,** *445* (4-6), 340-344.

[37] Assefa, Z.; Shankle, G.; Patterson, H. H.; Reynolds, R. "Photoluminescence studies of lanthanide ion complexes of gold and silver dicyanides: a new low-dimensional solid

state class for nonradiative excited-state energy transfer." *Inorg. Chem.* **1994,** *33* (10), 2187-2195.

[38] Bunzli, J.-C. G.; Comby, S.; Chauvin, A.-S.; Vandevyver, C. D. B. "New Opportunities for Lanthanide Luminescence." *J. Rare Earths* **2007,** *25* (3), 257-274.

[39] Petrova, J.; Haupt, E. T. K.; Momchilova, S.; Zdravkova, Z. "Lanthanide complexes with phosphine oxide and phosphonate ligands." *Synth. React. Inorg., Met.-Org., Nano-Met. Chem.* **1999,** *29*, 1641-1654.

[40] Iwanaga, H. "Development of novel rare-earth complexes and their application to emission devices." *J. Photopolym. Sci. Technol.* **2008,** *21*, 165-172.

[41] Sykora, R. University of South Alabama, personal communication